JGR Oceans

RESEARCH ARTICLE
10.1029/2024JC021702

Seasonal Source Water Changes and Winds Contribute to the Development of Hypoxia in St Helena Bay Within the Southern Benguela Upwelling System

A. J. Carlson[1], S. A. Siedlecki[1], J. Granger[1], J. Veitch[2,3], G. C. Pitcher[4,5], G. Fearon[2], F. Soares[1], M. Zhou[1], R. F. Flynn[6,7], and S. E. Fawcett[6,8]

[1]Department of Marine Sciences, University of Connecticut, Groton, CT, USA, [2]South African Environmental Observation Network (SAEON), Cape Town, South Africa, [3]Nansen-Tutu Center, Marine Research Institute, Department of Oceanography, University of Cape Town, Cape Town, South Africa, [4]Department of Forestry, Fisheries and the Environment, Cape Town, South Africa, [5]Department of Biological Sciences, University of Cape Town, Cape Town, South Africa, [6]Department of Oceanography, University of Cape Town, Cape Town, South Africa, [7]Earth, Marine and Environmental Sciences Department, University of North Carolina at Chapel Hill, Chapel Hill, NC, USA, [8]Marine and Antarctic Research Centre for Innovation and Sustainability (MARIS), University of Cape Town, Cape Town, South Africa

Abstract St Helena Bay (SHB), a retentive zone in the productive southern Benguela Upwelling System off western South Africa, experiences seasonal hypoxia and episodic anoxic events that threaten local fisheries. To understand the drivers of oxygen variability in SHB, we queried 25 years of dissolved oxygen (DO) observations alongside high-resolution wind and hydrographic data, and dynamical data from a high-resolution model. At 70 m in SHB (mid-bay), upwelling-favorable winds in spring drove replenishment of cold, oxygenated water. Hypoxia developed in summer, becoming most severe in autumn. Bottom waters in autumn were replenished with warmer, less oxygenated water than in spring—suggesting a seasonal change in source waters upwelled into the bay. Downwelling and deep mixing in winter ventilated mid-bay bottom waters, which reverted to hypoxic conditions during wind relaxations and reversals. In the nearshore (20 m), hypoxia occurred specifically during periods of upwelling-favorable wind stress and was most severe in autumn. Using a statistical model, we extended basic hydrographic observations to nitrate and DO concentrations and developed metrics to identify the accumulation of excess nutrients on the shelf and nitrogen-loss to denitrification, both of which were most prominent in autumn. A correspondence of the biogeochemical properties of hypoxic waters at 20 m to those at 70 m implicates the latter as the source waters upwelled inshore in autumn. We conclude that wind-driven upwelling drives the replenishment of respired bottom waters in SHB with oxygenated waters, noting that less-oxygenated water is imported later in the upwelling season, which exacerbates hypoxia.

Plain Language Summary St Helena Bay, in the southern Benguela Upwelling System off South Africa's west coast, experiences seasonal low oxygen and episodic anoxic events that threaten fisheries. We queried 25 years of dissolved oxygen observations in relation to wind data, simulations, and hydrographic data. Mid-bay winds bring off-shelf waters onto the shelf, which provide replenishment of cold, oxygenated bottom waters in spring. Winds drive ventilation in mid-bay waters, which return to low oxygen conditions during wind relaxations and reversals. In the nearshore, we found that oxygen was responsive to winds. Using a statistical model, we developed new metrics that identify periods of on-shelf nutrient retention relative to offshore waters, with increasing on-shelf accumulation of nutrients identified later in the season. This indicates source waters for upwelling change seasonally, with the spring supplying offshore water while later in the season, source waters are on-shelf. Hypoxia is most severe during autumn in the shallowest region of the shelf. In autumn, the properties of the shallow water explored here identify a correspondence with mid-bay water suggesting that on-shelf mid-bay water serves as a source of upwelled water to the shallow regions of the shelf. We conclude that winds bring offshore water which replenish low oxygen waters in SHB with oxygenated water in spring, but less oxygenated water later in the upwelling season, thus exacerbating autumn inshore low oxygen conditions.

Key Points:

- Nearshore hypoxia is most frequent during the late upwelling season, highly responsive to winds and likely sourced from mid-bay waters
- Seasonally varying ventilation pathways re-oxygenate mid-bay waters during spring upwelling as well as winter downwelling
- Nutrient trapping evolves seasonally, with nitrogen loss to denitrification in the autumn providing a potential negative feedback

Supporting Information:

Supporting Information may be found in the online version of this article.

Correspondence to:

S. A. Siedlecki,
samantha.siedlecki@uconn.edu

Citation:

Carlson, A. J., Siedlecki, S. A., Granger, J., Veitch, J., Pitcher, G. C., Fearon, G., et al. (2025). Seasonal source water changes and winds contribute to the development of hypoxia in St Helena Bay within the southern Benguela upwelling system. *Journal of Geophysical Research: Oceans*, *130*, e2024JC021702. https://doi.org/10.1029/2024JC021702

Received 9 AUG 2024
Accepted 6 MAR 2025

Author Contributions:

Conceptualization: A. J. Carlson, S. A. Siedlecki, J. Granger
Data curation: A. J. Carlson, S. A. Siedlecki, J. Veitch, G. C. Pitcher, G. Fearon, F. Soares, R. F. Flynn, S. E. Fawcett
Formal analysis: A. J. Carlson, S. A. Siedlecki, G. C. Pitcher, M. Zhou
Funding acquisition: S. A. Siedlecki, J. Granger, J. Veitch, S. E. Fawcett
Investigation: S. A. Siedlecki, J. Granger, J. Veitch, R. F. Flynn
Methodology: A. J. Carlson, S. A. Siedlecki, J. Granger
Project administration: S. A. Siedlecki, J. Granger
Resources: S. A. Siedlecki, J. Granger
Software: A. J. Carlson, G. Fearon
Supervision: S. A. Siedlecki
Validation: A. J. Carlson, S. A. Siedlecki

1. Introduction

Dissolved oxygen (DO) is declining globally (Breitburg et al., 2018; Diaz & Rosenberg, 2008; Laffoley & Baxter, 2019; Pitcher et al., 2021; Schmidtko et al., 2017) and hypoxia is becoming more widespread in coastal waters, with dire implications for productive coastal ecosystems. Prognostic information on the regional and

Writing – original draft: A. J. Carlson, S. A. Siedlecki, J. Granger
Writing – review & editing: A. J. Carlson, S. A. Siedlecki, J. Granger, J. Veitch, G. C. Pitcher, G. Fearon, F. Soares, M. Zhou, R. F. Flynn, S. E. Fawcett

global drivers of hypoxic events is critical if the communities reliant on these ecosystems are to adapt and respond to their changing ocean. The southern Benguela Upwelling System (SBUS), located along the west coast of southern Africa, is one of the major Eastern Boundary Upwelling Systems. In spring and summer, equatorward winds drive upwelling of nutrient-rich cold water onto the shelf, promoting high biological productivity that fuels socioeconomically important fisheries (Nelson & Hutchings, 1983). In winter, by contrast, upwelling is dampened due to seasonal changes in the strength and direction of the winds (Hutchings et al., 2009a, 2009b). The region is also characterized by seasonal hypoxia (i.e., dissolved oxygen depletion [O_2] $\leq$ 60 μm), which is generally most severe in St Helena Bay (SHB), a retentive "upwelling shadow" zone in the SBUS (Bailey & Chapman, 1985, 1991; de Decker, 1970; Demarcq et al., 2007; Flynn et al., 2020; Huggett et al., 2009; Jarre et al., 2015; Largier, 2020; Lett et al., 2006; Monteiro & van der Plas, 2006; Pitcher et al., 2014, 2022; Pitcher & Probyn, 2017; Weeks et al., 2006). The lower energy environment of the bay, particularly during summer, provides conditions that favor the development of large phytoplankton blooms (Demarcq et al., 2007; Pitcher et al., 1998; Probyn et al., 2000; Weeks et al., 2006). The decay of these blooms results in the progressive decline of bottom water oxygen throughout the upwelling season, culminating in severely depleted dissolved oxygen concentrations (≤20 μm) in late summer (Pitcher et al., 1998; Probyn et al., 2000). Mass walkouts of rock lobsters along the west coast of South Africa have occurred coincident with incidences of lowest oxygen, which appears linked to the development and subsequent decay of high-biomass harmful algal blooms (Cockcroft et al., 2008; Pitcher & Jacinto, 2019).

Oxygen depletion in SHB—and throughout the SBUS more generally—is considered a consequence of local processes (Bailey, 1991; Flynn et al., 2020; Monteiro & van der Plas, 2006). The persistent seasonal hypoxia at the subsurface of the bay is cited to evolve from a confluence of factors. First, periods of upwelling-favorable winds drive the entrainment of nutrient-rich water onshore, leading to high productivity (Nelson & Hutchings, 1983). The consequent export of organic carbon to the shallow shelf incurs a high oxygen demand at the subsurface (Hutchings, Roberts, & Verheye, 2009). Repeated cycles of production and remineralization promote the accrual of subsurface nutrients throughout the upwelling season and the concomitant depletion of dissolved oxygen (Flynn et al., 2020). Second, summer stratification, which develops in the bay during wind relaxations, impedes ventilation by downward mixing (Nelson & Hutchings, 1983), although strong diurnal-inertial oscillations driven by the land-sea breeze facilitate pycnocline outcropping and diapycnal mixing through much of the summer (Burger et al., 2020; Fearon et al., 2020; Lucas et al., 2014). Finally, the replenishment of bottom waters is cited to be low due to the retentive properties of SHB (Penven et al., 2000), hindering ventilation of the subsurface (Bailey & Chapman, 1991; Pitcher et al., 2014; Pitcher & Probyn, 2017).

The hydrodynamic processes in the bay are governed by the prevailing wind (Holden, 1985; Penven et al., 2000; Pitcher et al., 1998; Pitcher & Probyn, 2017), the seasonal and synoptic variations of which determine current flow and associated changes in water column structure. A prognostic understanding of these inter-connected drivers remains elusive, however, precluding anticipation of the onset and severity of hypoxic events. Previous work identified that the severity of hypoxia is related to the number of upwelling days during the summer and the total upwelling divergence (Jarre et al., 2015). Subsequently, Flynn et al. (2020) advanced that thermal fronts and associated jets borne of seasonal upwelling cause the onshore retention of upwelled waters, promoting the on-shelf accrual of regenerated nutrients in excess of concentrations in the upwelled source waters (i.e., nutrient trapping) and the consequent depletion of oxygen. A multi-decadal trend in upwelling favorable winds has been identified in the SBUS (Lamont et al., 2018) alongside a cooling trend in SST (Rouault et al., 2010). Although the implications for SBUS oxygen are as-yet unknown, climate change is expected to drive an increase in wind intensity at the poleward edges of all Eastern Boundary upwelling regions (Rykaczewski et al., 2015; Sydeman et al., 2014), potentially modifying patterns in SBUS shelf hypoxia.

To develop a mechanistic understanding of the drivers and local modifiers of hypoxia in SHB, we characterize the relationship between wind-driven upwelling dynamics, dissolved oxygen, and subsurface nutrient concentrations. Through the development of new metrics that rely on a statistical model that extends basic local hydrographic observations to oxygen concentrations and nutrients, we identify periods when nutrients accumulate on the shelf in excess of those in the upwelled source waters. We use these metrics alongside multiple data sources including model output to diagnose the origins of the seasonal water supply to the mid- and nearshore regions of SHB. Our study reveals strong correspondence of dissolved oxygen dynamics to incident wind stress, nuanced by differences in seasonal ventilation pathways. We also find evidence of onshore nutrient trapping year-round and interannually along the St Helena Bay Monitoring Line and identify a seasonal pattern for the negative feedback to

nutrient trapping, with important implications for the fate of the trapped nutrients. Our results provide insight into the drivers and potential mechanisms of nearshore hypoxia in SHB.

1.1. Study Area

The SBUS extends along the west coast of southern Africa, demarcated hydrographically from the northern Benguela Upwelling System by a perennial upwelling cell at Lüderitz (~27°S; Duncombe Rae, 2005; Hutchings, van der Lingen, et al., 2009; Lett et al., 2007). Equatorward winds, enhanced wind stress curl, coastline orientation, and local narrowing of the shelf in the vicinity of the discrete upwelling cells of the Cape Peninsula (34°S), Cape Columbine (33°S), Namaqualand (30°S), and Lüderitz drive offshore Ekman transport of surface waters from spring through autumn. The associated upwelling of cold water nearshore sets up a shelf edge front that extends from Cape Columbine and is referred to as the Columbine upwelling cell. An associated equatorward jet (the Cape Jet (CJ) or Goodhope Jet) bifurcates north of Cape Columbine into an offshore (Shelf Break Front; SBF) and alongshore (Columbine Front; CF) component (Lamont et al., 2015). The latter acts as a dynamic boundary between SHB and waters offshore (Lamont et al., 2015), leading to a cyclonic retentive flow in the bay (Penven et al., 2000). During the upwelling season, typically from October to April (Lamont et al., 2015), Subantarctic Mode Water (SAMW) and overlying South Atlantic Subtropical Mode Water (SASTMW) upwell onto the shelf inshore of the CF (Flynn et al., 2020; Lamont et al., 2015; Tim et al., 2018). SAMW occupies the off-shelf water column between roughly 200 and 400 m and is present on-shelf year-round (Flynn et al., 2020; Lamont et al., 2015). SASTMW is less dense than SAMW, occupying the water column off-shelf between 80 and 200 m, and has been observed east of the CJ and CF (Flynn et al., 2020; Lamont et al., 2015). These source waters are well oxygenated from recent ventilation in the Southern Ocean and are relatively nutrient-rich. The chemical properties of source waters retained on the shelf are modified substantially from repeated upwelling-related cycles of production and remineralization, resulting in the accrual of subsurface nutrients on the shelf and an associated decline of oxygen, with extreme hypoxia observed in SHB (Bailey, 1987; Calvert & Price, 1971; Flynn et al., 2020; Tyrell & Lucas, 2002).

2. Materials and Methods

2.1. Data Sets

We collated existing observational data sets of pertinent regional hydrographic variables, including depth profiles of temperature (T), salinity (S), nitrate concentrations (N), and dissolved oxygen concentrations (DO) (Table S1 in Supporting Information S1). Data sets originate from the CLIVAR A-10 and A-10.5 lines, the St Helena Bay Monitoring Line (SHBML), and the Department of Forestry, Fisheries and the Environment (DFFE) Integrated Ecosystem Program (IEP) cruises. The SHBML data were collected at quasi-monthly intervals from 2000 to 2014, whereas the IEP data were collected at seasonal intervals from 2017 to 2022. Climatologies from the SHBML were also used in our analysis (de Villiers, 2017).

We also investigated observations of T, S, and DO from a mooring deployed at 20 m depth within SHB off Elands Bay (32.292°S, 18.318°E) from November 2008 to December 2011, and from a 70 m mooring deployed in SHB (32.329°S, 18.183°E) from January 2012 to December 2012 (Pitcher et al., 2014; Pitcher & Probyn, 2011; Table S1 in Supporting Information S1 and Figure 1). Time-series data were filtered to account for the tidal signal and then binned into daily averages.

To investigate drivers of hydrochemical properties at the moored sites, we applied a new atmospheric product developed as part of the Wind Atlas for South Africa (WASA) project (Lennard et al., 2015). Here, we explore both the alongshore wind stress as well as the wind stress curl from WASA, which was not available in previous observational analyses and is higher resolution (3 km) than prior products. We explore both wind stress and wind curl because both have been shown to matter in this region for oxygen (Jarre et al., 2015; Pitcher et al., 2014; Pitcher & Probyn, 2017). We expect this product to resolve the impact of the headland locally on the winds. We only use the winds within the basin, not the regional average, which likely includes the effect of headlands on the local wind field within. Using the WASA wind product, we derive the alongshore wind stress (AWS) at the site of the 20 m mooring and to compute the wind stress curl at the 20 and 70 m mooring locations. CROCO simulations write out the wind stress from the simulation in both the u and v directions. The CROCO grid is approximately aligned with the shoreline; therefore, here we used the v direction (north-south orientation) which is tied to the

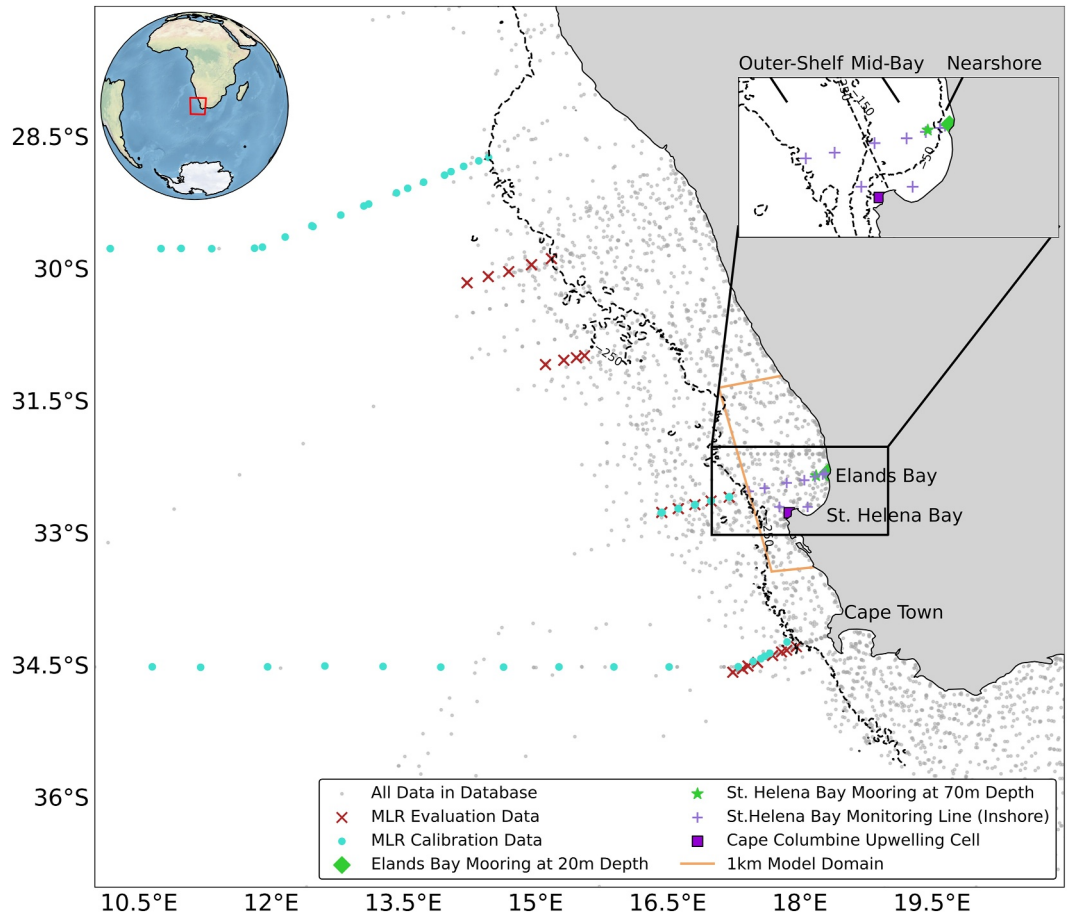

Figure 1. Map of the southern Benguela Upwelling System, off the west coast of South Africa, showing the observational hydrographic stations and model domains used in this study. The data used to calibrate the multiple linear regressions (MLRs) are from locations indicated by aqua circles, MLR evaluation data are from positions marked by red x's, mooring data locations are shown by the green diamond (20 m) and green star markers (70 m), and the inshore St Helena Bay stations are denoted by the purple plus sign markers. The 1 km model domain is shown by the solid orange line. The shelf break is denoted by the dashed line (250 m) on the main map, whereas different regions of the shelf (nearshore, mid-bay, and outer-shelf) are separated in the inset map by the 50 m (nearshore), 150 m (mid-bay), and 250 m (outer-shelf) isobaths, respectively.

grid, for the AWS. For the Cape Columbine cell, an approximate location of [32.75°S, 17.88°E] was used for the computations (Figure 1). The wind stress curl (WSC) was calculated as:

$$WSC = \frac{\partial \tau_y}{\partial x} - \frac{\partial \tau_x}{\partial y} \quad (1)$$

where τ_x and τ_y are the wind stress components along x (eastward) and y (northward) directions.

We also extracted complementary physical (T and S) and dynamical data at the mooring sites from daily averaged output from a high-resolution (1 km), 2-way nested dynamical ocean model of SHB (Fearon et al., 2023). The model code is based on the V1.0 release of the Coastal and Regional Ocean Community model (CROCO). The parent domain focuses on the region from 30 to 35°S and 16–19°E, whereas the child domain focuses on SHB from 32.35 to 33.3°S and 17.2–18.4°E. The model bathymetry was generated based on data provided by the South African Navy. The oceanic boundary conditions for the parent domain were based on a 1/12° global ocean reanalysis product provided by the HYCOM consortium (https://www.hycom.org/data/glbu0pt08/expt-19pt1) and atmospheric forcing was obtained from the 3 km resolution WASA atmospheric product (Lennard et al., 2015). Model output corresponding to the mooring locations was extracted from the closest model grid cell

in space and time. More information about the construction and validation of this model can be found in Fearon et al. (2023).

The vertical velocity at the base of the Ekman Layer, presumed here to be at a water depth of 10 m, was extracted from the regional model simulation. This metric was integrated over the active zone of upwelling, about 10 km perpendicular to the coastline in this region (Veitch et al., 2009), in order to quantify vertical transport. This metric is referred to here as velocity-based transport (VBT) and calculated as follows:

$$\text{Velocity Based Transport}\left(\vec{V}\right) = \int_{\text{x=10 km offshore}}^{\text{x=mooring}} w \ \text{dx} \tag{2}$$

where w = modeled vertical velocity (at the base of the Ekman layer, L_0 = 10 km) and dx = 1 km (width of one grid cell).

We also estimated the mixed layer depth at the site of the 70 m mooring from the CROCO simulation using the method described in Lorbacher et al. (2006) from the CROCO tools (Penven et al., 2022). The mixed layer depth at each time step was identified as the shallowest extreme curvature of near surface layer temperature profiles that are closest to the 70 m mooring.

2.2. Multiple Linear Regression (MLR) Development

We developed MLR models to predict interannual changes in the chemistry of source water masses from the collection of observational data sets described above. These models were used to investigate the evolution of shelf biogeochemical properties relative to source waters offshore using regional hydrographic data sets (Table S1 in Supporting Information S1). The TEOS-10 system (IOC et al., 2010) from the Gibbs-SeaWater (GSW) toolbox for Python (McDougall & Barker, 2011) and T and S were used to compute the corresponding density (D). T, S, and D were then used to predict nitrate (N) and DO concentrations, as well as apparent oxygen utilization (AOU), in the source waters that are upwelled onto the shelf (Section S2 and Table S3 in Supporting Information S1). Apparent oxygen utilization is defined as the difference between the DO at saturation conditions defined by observed salinity and temperature and the observed DO (Weiss, 1970). Here, AOU was derived from measured DO and estimates of oxygen saturation calculated using the GSW toolbox from observed T and S (McDougall & Barker, 2011). Observations were sorted to target modified waters offshore of the 250 m isobath and were isolated between 50 and 600 m depth. Co-located observations of T, S, DO, and N for a given date, depth, and location were selected from within the spatial bounds of 10°E–20°E and 28°S–36°S. Data from the CLIVAR and SHBML efforts were used to calibrate the MLRs (n = 371), whereas the 2017 IEP cruise data were retained for independent evaluation of the MLRs (n = 342) (Table S1 in Supporting Information S1).

The variance inflation factor (VIF) was used to assess collinearity among the predictor variables (T/S/D for the N MLR and N/T/S/D for the DO and AOU MLRs). Combinations of predictor variables resulting in VIF scores greater than 10 were excluded from further analysis to minimize the variance of the regression coefficients caused by co-linearity (Kutner et al., 2004). Models with a lower Akaike Information Criterion (AIC), which indicates lower prediction error and model complexity, were ultimately selected (Akaike, 2011, Table 1).

2.3. Metrics Used in MLR Application to Assess St Helena Bay Dynamics

Data from the SHBML were compared to MLR-predicted source water values to investigate the evolution of chemical properties inshore of the 250 m isobath (Table S1 in Supporting Information S1). Riverine input to SHB is negligible (Pitcher et al., 2023; Pitcher & Probyn, 2017); as such, our analysis does not consider anthropogenic river-borne nutrients.

To identify non-conservative changes in nitrate concentrations inshore of 250 m, we computed the difference between the observed nitrate concentration and the MLR-predicted source water values, termed here as ΔNO_3^-:

$$\Delta NO_3^-\left(\mu\text{molkg}^{-1}\right) = [NO_3^-\text{Observations}] - [NO_3^-\text{MLRpredicted}] \tag{3}$$

Changes in AOU compared to source waters were also computed, with ΔAOU calculated as the difference between the observed and MLR-predicted source water AOU:

$$\Delta\text{AOU}\left(\mu\text{mol kg}^{-1}\right) = [\text{AOU Observations}] - [\text{AOU MLRpredicted}] \quad (4)$$

2.4. Regional Data Analysis

The derived biogeochemical parameters, ΔNO_3^- and ΔAOU, are separated by season: spring (September, October, and November), summer (December, January, and February), autumn (March, April, and May), and winter (June, July, and August). In addition, some results are divided into the 'upwelling season', which includes data from October through to April, and the 'winter season', which includes data from June through September. Because of the unique physical dynamics, including upwelling over a broad shelf alongside a recirculation cell within SHB, the data were divided into depth bins to isolate signals specific to the different shelf regions (Figure 1). The nearshore region encompasses data from shallower than the 50 m isobath, the maximum seasonal average mixed layer depth (MLD) in the region (Russo et al., 2022), and includes the 20 m mooring (Pitcher et al., 2014; Pitcher & Probyn, 2011), the model output from the 20 m mooring location (Fearon et al., 2023), and the SHBML stations 1, 2, and 21. The goal of defining this bin was to isolate that part of SHB influenced by weak, wind-driven upwelling near Elands Bay in the region of the inner shelf upwelling front. It is worth noting that the region where the 20 m mooring resides, which we refer to as nearshore, is subject to a narrow belt of upwelling and responds to alongshore wind stress in a 2-D sense (Pitcher & Probyn, 2017). The mid-bay region incorporates data from between the 50 and 150 m isobaths, and includes the 70 m mooring (Pitcher et al., 2014; Pitcher & Probyn, 2011), the model output from the 70 m mooring location (Fearon et al., 2023), and the SHBML stations 3, 4, 5, and 22. Here, the aim was to isolate that part of SHB influenced by the retention cell. The outer-shelf region incorporates data from between the 150 and 250 m isobaths and includes the model output from the approximate center of the Cape Columbine upwelling cell [32.75°S, 17.88°E] location (Figure 1; Fearon et al., 2020) and the SHBML stations 6 and 7. This bin isolated the major upwelling signal at Cape Columbine which, depending on the time of year, can further isolate SHB from the rest of the shelf.

To assess the influence of the winds, a regression analysis was performed comparing the model derived upwelling indices (VBT, ASW, and WSC) to both the model and observed bottom-water T and DO records from the mooring locations, which notably span a shorter period of time than the SHBML in situ observations (Table S1 in Supporting Information S1). Time-series of ocean conditions and winds were smoothed using a running 7-day average to focus on event-scale variability. The SciPy package in Python was used to calculate the correlations, specifically the linregress() function without any customization. The same package was used to compute the p-values as well without consideration of serial correlation between two different time series as large-scale physical oscillations and seasonality were a desired inclusion. For all the averages reported here, each individual observation was treated independently and the number of observations (n) during each time-averaged interval is included in the results tables for reference.

3. Results

3.1. MLR—Model Selection, Structure, and Performance

Statistical models for source water DO (MLR_{DO}), AOU (MLR_{AOU}), and N (MLR_N) were generated from in situ observations from the SBUS. A full accounting of these equations and relevant statistics can be found in Table 1. The models for DO and AOU considered T, S, D, and N as potential predictors, whereas the models for N considered only T, S, and D as potential predictors. To predict N (MLR_N), a MLR based on T only was chosen from allowed predictors (Figure 2a). The MLR_N performed well against both the calibration data ($R^2 = 0.82$) and the evaluation data ($R^2 = 0.89$, Figure 2a). Both the AOU (MLR_{AOU}) and DO (MLR_{DO}) MLRs chosen are a linear combination of S, N, and D. Dissolved oxygen and AOU in the source waters were both well simulated with the MLRs generated, but AOU performed the best in terms of R^2 when compared to the evaluation data (Table 1). The MLR_{DO} performed fairly against both the calibration ($R^2 = 0.45$) and evaluation data ($R^2 = 0.46$; Figure 2b). The MLR_{AOU} performed well against the calibration data ($R^2 = 0.73$) and better against evaluation data ($R^2 = 0.81$, Figure 2c). Consequently, the MLR_{AOU} was selected for our analysis rather than the MLR_{DO}. The MLRs capture the variability of all the calibration data for each predicted variable (DO, AOU, and N), and as such, simulate interannual variability in source waters in the region.

Journal of Geophysical Research: Oceans

10.1029/2024JC021702

Table 1
Multiple Linear Regression Equations and Statistics Using All Calibration and Evaluation Data Noted in Figure 1

	Dependent variable	Equation	Calibration adjusted R^2	Calibration RMSE	Δ AIC	Coeffs ± std. error	Evaluation adjusted R2	Nested MLR R^2	Climatology MLR R^2
Calibration: 371 Evaluation: 342	Oxygen	$a_0 + a_1{*}S + a_2{*}N + a_3{*}D$	0.45	22.5	0	$a_0 = -13079 \pm 2782.1$ $a_1 = -13.495 \pm -3.8657$ $a_2 = -3.8657 \pm 0.29516$ $a_3 = 13.442 \pm 2.5178$	0.46	0.32	0.01
	AOU	$a_0 + a_1{*}S + a_2{*}N + a_3{*}D$	0.73	22.5	0	$a_0 = 10{,}273 \pm 2788.2$ $a_1 = -28.125 \pm 8.9228$ $a_2 = 4.024 \pm 0.2958$ $a_3 = -9.0376 \pm 2.5233$	0.81	0.77	0.28
	Nitrate	$a_0 + a_1{*}T$	0.82	3.8	0	$a_0 = 41.313 \pm 0.65897$ $a_1 = -2.2964 \pm 0.056878$	0.89	_	_

Note. The calibration data set had 371 values, and the evaluation data set had 342 values.

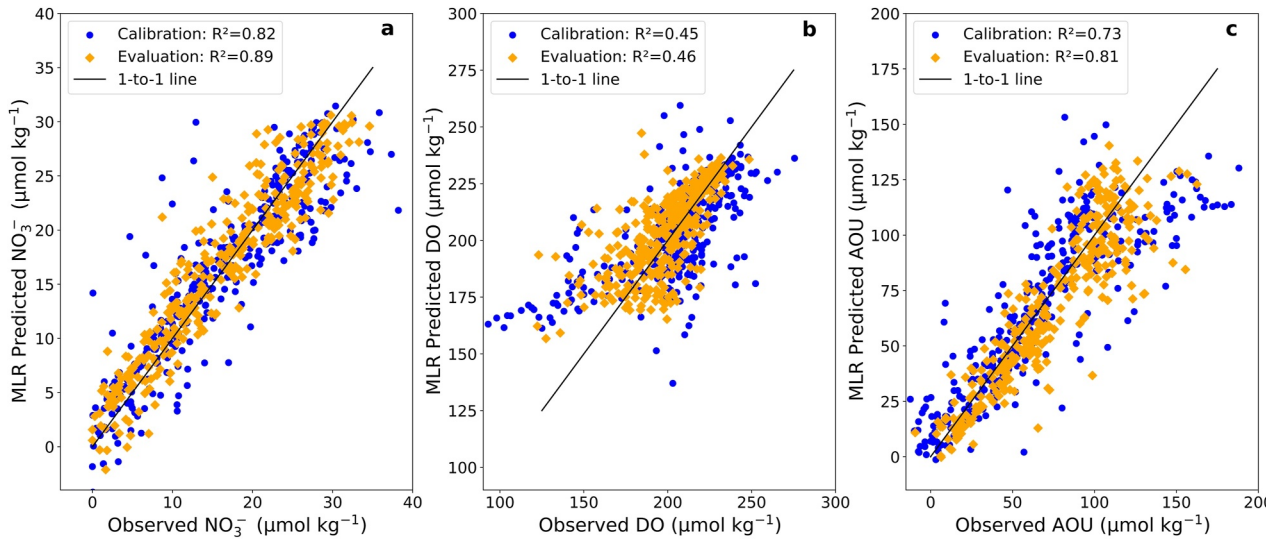

Figure 2. Scatter plots of the model calibration (blue circles) and evaluation (orange diamonds) results compared to observations of SBUS source waters for (a) nitrate (NO_3^-), (b) dissolved oxygen (DO), and (c) apparent oxygen utilization (AOU). The observations are plotted along the *x*-axis and MLR predicted concentrations along the *y*-axis. Coefficients of determination are provided in the subfigure legend and in Table 1.

3.2. Wind-Driven Variability

3.2.1. Wind Analysis

Over the simulated period (2008–2012), the alongshore winds at the location of the 20 m mooring were dominantly upwelling-favorable in spring through autumn, with mean values (averaged over upwelling-favorable periods only) of 0.19 N m^{-2} during spring, 0.20 N m^{-2} in summer, and 0.13 N m^{-2} in autumn (Table 2). Upwelling-favorable winds were less frequent during winter and of lower amplitude than during the other seasons (mean of 0.11 N m^{-2}). The alongshore winds were dominantly downwelling-favorable during winter, with a mean amplitude of −0.22 N m^{-2}, comparable to downwelling wind strengths observed during autumn (mean of −0.23 N m^{-2}). Downwelling-favorable winds were weaker during spring (mean of −0.14 N m^{-2}) and weakest in summer (mean of −0.08 N m^{-2}).

3.2.2. Relationship of DO and T to Wind Variability in the Mid-Bay

DO concentrations at 70 m in SHB ranged from 5 to 240 µmol kg^{-1} (Figure 4). In general, normoxic conditions occurred as seasonal upwelling began. DO concentrations decreased rapidly thereafter, reaching hypoxic

Table 2
Seasonal Descriptive Statistics for Alongshore Wind Stress (AWS) From Paired Model and Moored Observations in the Nearshore Region (N m^{-2}) Where the Winds Were Separated Into Seasons and Examined According to Wind Direction (i.e., Upwelling or Downwelling Favorable)

Metric	Season	Direction	Min	Max	Median	Average	Obs # (n)
AWS	Spring	Upwelling	9.90E−05	4.54E−02	1.90E−02	1.90E−02	157
		Downwelling	−3.50E−02	−8.60E−05	−1.20E−02	−1.42E−02	56
	Summer	Upwelling	1.90E−03	3.70E−02	2.09E−02	2.02E−02	113
		Downwelling	−1.99E−02	−3.16E−04	−4.26E−03	−7.79E−03	8
	Autumn	Upwelling	4.91E−04	4.20E−02	1.09E−02	1.30E−02	178
		Downwelling	−8.20E−02	−4.79E−04	−1.65E−02	−2.31E−02	80
	Winter	Upwelling	1.03E−04	3.66E−02	1.01E−02	1.17E−02	57
		Downwelling	−8.96E−02	−2.00E−06	−1.80E−02	−2.18E−02	210

Note. The observation number (n) identifies the weekly averaged events observed during each season.

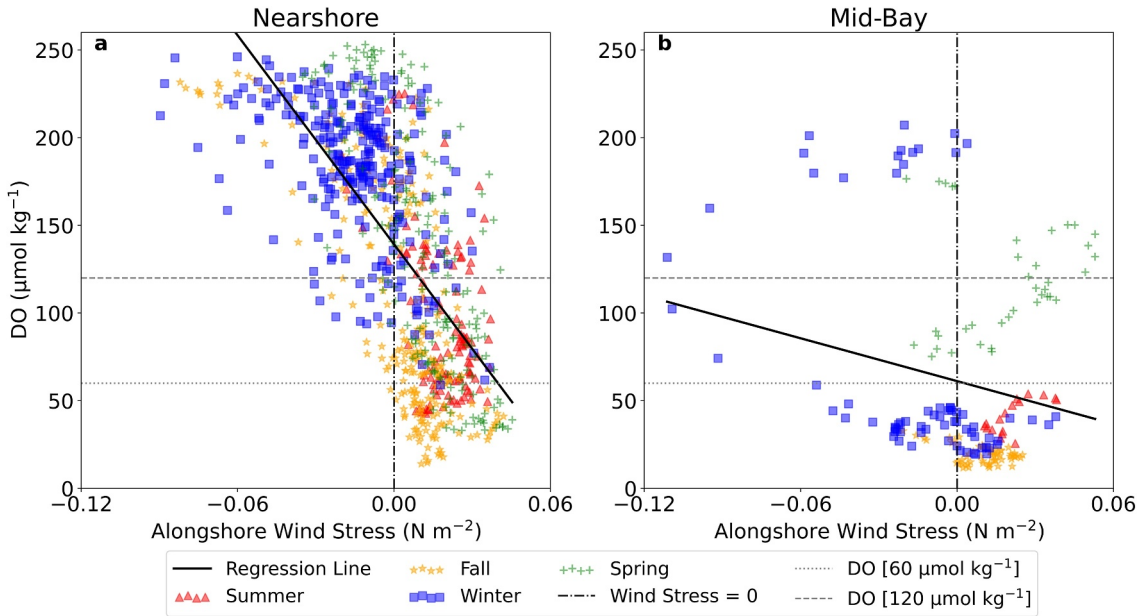

Figure 3. Dissolved oxygen (DO) concentrations in relation to alongshore wind stress (AWS) from (a) the 20 m mooring and (b) the 70m mooring (DO from Pitcher & Probyn, 2011; Pitcher et al., 2014). The hypoxia threshold is shown by the dotted horizontal line (60 μmol kg^{-1}) and the oxygen deficiency threshold by the dashed horizontal line (120 μmol kg^{-1}). The different colors and symbols indicate the different seasons (red triangle—summer, blue square—winter, orange star—autumn, and green cross—spring). AWS = 0 N m^{-2} is indicated by the vertical dash-dotted line and the regression of DO on AWS for each regional data set (all seasons) is shown by the solid black line.

conditions in summer through autumn, with the lowest DO generally occurring during autumn. The mooring DO measurements were made at 1 m above the seafloor, whereas the CTD DO measurements were made 5–10 m off the seafloor, contributing to the occasional mismatch between the CTD and mooring data in Figures 4 and 5. Frequent multi-week ventilation events occurred in winter, which were punctuated by lower DO conditions.

Temperature at the 70 m mooring was relatively cold throughout the upwelling season at a median value of 9.5°C, increasing slightly from spring (9.2°C) to autumn (9.7°C). The T record during the upwelling season was punctuated by slight warming events that rarely exceeded 10.5°C—and were associated with slight DO increases. During winter, T at 70 m was generally warmer, ∼10°C, and revealed intermittent warming events that reached upwards of 12°C (and 14°C in simulations in years for which we have no observational data).

The relation of water T at 70 m to nearshore wind metrics at Elands Bay provides evidence of subsurface transport compensating for upwelling at the coast. Temperature at the 70 m mooring was inversely correlated with AWS inshore at Elands Bay year-round (R^2AWS = 0.38, Table 3b) and directly correlated with the WSC (R^2WSC = 0.41). These associations suggest that upwelling inshore leads to the entrainment of colder water at 70 m in SHB. On a seasonal basis, wind metrics nearshore explained substantially less of the variability in T in winter ($R^2 = 0.12$ for ASW, and no significant correlation with WSC) than during other seasons ($R^2 = 0.36$ to 0.53 for ASW), suggesting a process other than winds is important for oxygen variability in winter.

The relationship between DO and inshore upwelling metrics at the 70 m mooring proved complex, revealing contrasting seasonal patterns. In spring, DO was not significantly related to the wind metrics (Table 3), potentially due to the larger variability in the observations during this season making significant relationships more difficult to observe in this relatively short coastal data set. However, DO was insignificantly positively correlated with co-located T ($R^2 = 0.14$, Table 3), suggesting an association of colder water with lower oxygen (Figures 4 and 6, Table 3) although an inverse relationship between DO and T is arguably apparent in Figure 6. Indeed, if alongshore wind stress was used to define upwelling transition, rather than rigid seasonal time blocks, the relationship between oxygen and temperature in spring is negative ($R^2 = 0.67$, not shown) and significant. DO in spring was not explained by the nearshore upwelling metrics nor by coincident T because of a seasonal reversal in the relationship between DO and T (Figure 6), owing in part to the entrainment of colder, more oxygenated water onshore, following the seasonal wind reversal in spring (Figure 6). Although colder water at 70 m was generally

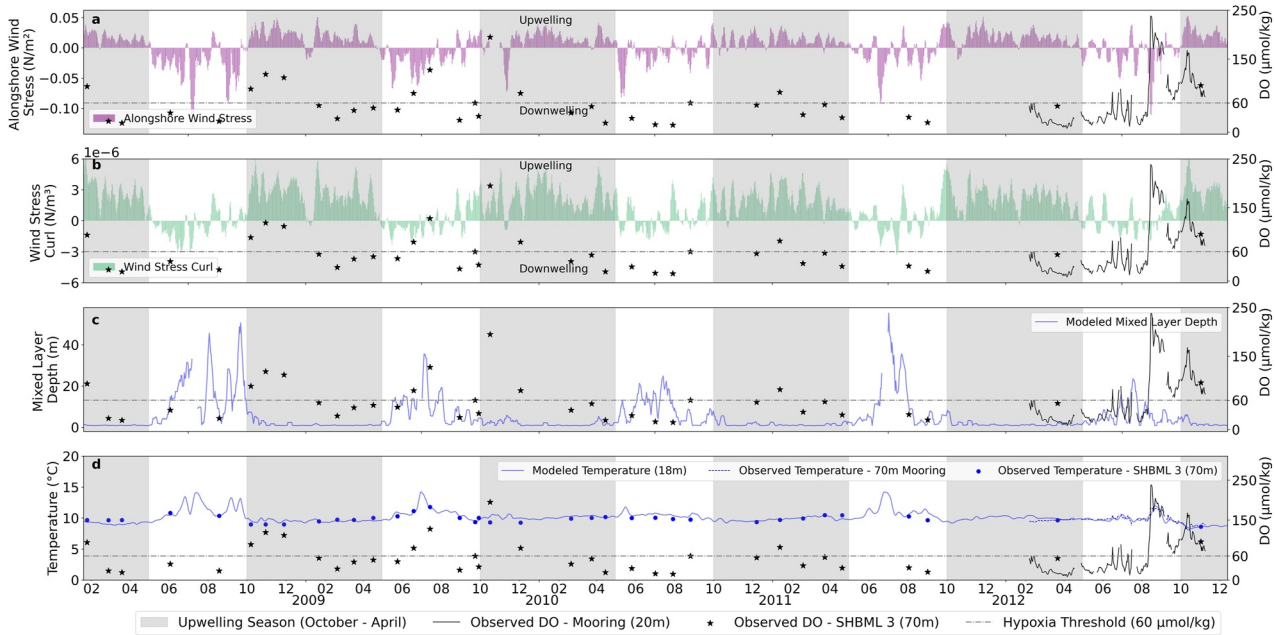

Figure 4. Time-series of dissolved oxygen (DO) data from 2008—2012 from the 70 m mooring [32.329°S, 18.183°E] (Pitcher et al., 2014; Pitcher & Probyn, 2011) and SHBML Station 3 at 70 m plotted in black lines and stars, respectively, along with model wind output at the site of the 20 m mooring [32.292°S, 18.318°E] showing (a) alongshore wind stress (AWS), (b) wind stress curl (WSC), (c) mixed layer depth (MLD), and (d) T. Gray shading indicates the upwelling season spanning from October to April. Positive values in the transport metrics and wind stress indicate upwelling favorable conditions, where $y = 0$ is indicated by the black line. The hypoxic threshold of 60 µmol/kg is indicated by the dotted black line.

associated with lower DO during late winter, cold yet higher DO water was upwelled onshelf during the spring transition (Figure 4).

During summer, the variability in DO at the 70 m mooring was in part explained by the AWS inshore at Elands Bay ($R^2_{ASW} = 0.50$; Table 3), wherein upwelling was associated with increased DO at 70 m. Water at the 70 m mooring was thus replenished by colder and more oxygenated water in summer, analogous to spring, albeit with a slope attesting to a lesser replenishment of cold water for a given alongshore upwelling wind strength. DO and T were inversely correlated in summer ($R^2T = 0.88$; Table 3) when upwelling entrains colder, more oxygenated water onshore. Small ventilation events throughout the upwelling season were generally associated with slight but detectable increases in bottom T, suggesting the incursion of warmer, DO-replete surface waters at these depths These small ventilation events visually coincided with relaxations in wind and vertical velocity in Elands Bay (Figure 4). In all, the observations evince two modes of ventilation at the 70 m mooring during summer: (a) the onshore entrainment of colder, more oxygenated water, and (b) the downwelling of warmer, more oxygenated surface waters likely originating nearshore.

During autumn, DO at the 70 m mooring was chronically low (Figure 4). The relationship between DO and upwelling metrics reversed from that observed in summer; the upwelling-favorable AWS (and the negative WSC) inshore was inversely correlated with DO at the 70 m mooring, albeit weakly ($R^2AWS = 0.18$, $R^2WSC = 0.15$, Table 3). Additionally, DO and T were only weakly positively correlated ($R^2_T = 0.06$; $p = 0.05$). Bottom waters were thus seemingly replenished by colder, yet *less* oxygenated water during upwelling events in autumn, in contrast to spring and summer when upwelling induced replenishment with more oxygenated water.

In winter, DO increased during both short-lived and multi-week ventilation events, before hypoxic conditions were re-established (Figure 4). DO and T were significantly inversely correlated to the AWS inshore at Elands Bay ($R^2 = 0.25$; $R^2 = 0.17$; Table 3)—although weakly so—but showed no correlation to the corresponding WSC. DO remained significantly positively correlated with T ($R^2 = 0.96$, Table 3). A large excursion in DO and corresponding T (up to 15°C) occurred in 2012, directly following a severe wind event (wind stress exceeding 1 N m^{-2}) with downwelling favorable alongshore winds, suggesting that bottom waters were ventilated by downwelling of nearshore waters, potentially as a consequence of severe winter storms. Estimates of MLD at the location of the 70 m mooring from the dynamical simulations suggest that it remained relatively shallow during

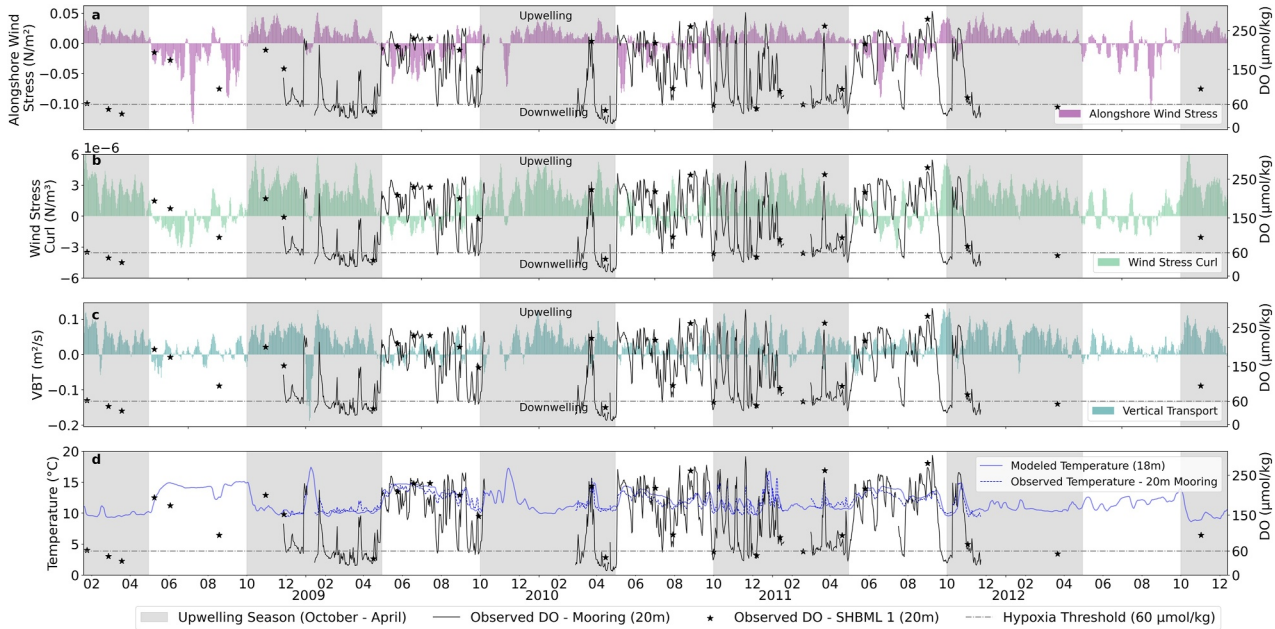

Figure 5. Time series of dissolved oxygen (DO), shown in black lines, from a mooring at 20 m in the Elands Bay region of St. Helena Bay [32.292°S, 18.318°E] from 2008—2012 (Pitcher et al., 2014; Pitcher & Probyn, 2011), and from the St Helena Bay Monitoring Line (SHBML) Station 1 at 20 m (black stars), plotted with a 7-day rolling average. Also shown is (a) alongshore wind stress, (b) wind stress curl, (c) velocity based transport (VBT), and (d) modeled and observed T. Wind metrics (a), (b) from WASA atmospheric product (Lennard et al., 2015) and water metrics (c), (d) from 1 km model output (Fearon et al., 2023). Gray shading indicates the upwelling season spanning October to April. Positive values in the transport metrics and wind stress indicate upwelling favorable conditions. The hypoxic threshold of 60 µmol/kg is indicated by the dotted black line.

this event (Figure 4), further arguing that downwelling in the nearshore region was the source of the warm surface water, rather than local mixing. In previous years for which we have a sparse observational record, positive T excursions from the dynamical simulations coincided with a deepening of the surface mixed layer to more than half the depth of the water column, suggesting that wind-driven deep local mixing may also provide a mechanism for ventilation;however, no DO observations exist during these simulated events to corroborate this dynamic. The SHBML data from near the 70 m mooring similarly suggest periods of ventilated waters interspersed with hypoxic conditions over the length of the observations (2000–2014).

3.2.3. Relationship of DO and T to Wind Variability in the Nearshore

DO concentrations from the 20 m mooring at Elands Bay and from CTD and bottle measurements inshore of the 50 m isobath from the SHBML revealed seasonal trends. Values in the nearshore region were generally lower in summer (20 m mooring median = 82.5 µmol kg^{-1} and SHBML median = 59.0 µmol kg^{-1}) and higher in winter (20 m mooring = 187.1 µmol kg^{-1} and SHBML = 218.0 µmol kg^{-1}; Figure 3). DO concentrations were directly correlated to T year-round (R^2 = 0.67; Table 3a), with lower concentrations associated with colder water, as documented previously by Pitcher and Probyn (2017). Both DO and T were highly responsive to upwelling metrics, decreasing during upwelling events as a function of upwelling-favorable AWS (R^2 = 0.47) and the negative wind stress curl (R^2 = 0.47). During the upwelling season, respective upwelling metrics explained more of the variance in DO and T during spring and autumn (R^2 = 0.39, 0.42 for T; R^2 = 0.56, 0.53 for DO; Table 3) than during summer (R^2 = 0.16 for T; R^2 = 0.23 for DO; Table 3).

During upwelling favorable conditions specifically, DO concentrations at the 20 m mooring were generally higher (average of 91.1 µmol kg^{-1}) earlier in summer than in autumn (Figure 5). Hypoxic conditions thus occurred predominantly during the latter part of the upwelling season but were rapidly mixed away during ventilation events. Ventilation events during the upwelling season corresponded to slight wind relaxations, evinced by reversals from upwelling-to downwelling-favorable AWS and a reduced WSC and VBT. These events coincided with slight increases in T (≤1°C) from median values of ~10°C. A few ventilation events during the upwelling season were associated with net downwelling as evidenced from concurrently large increases in water

Table 3

Correlations of Moored Measurements of DO and Modeled T at (a) 20 m in Elands Bay [32.292°S, 18.318°E] and Observed DO and T From February–November 2012 at (b) 70 m in St Helena Bay [32.329°S, 18.183°E], Against Upwelling Indices at Elands Bay Derived From the WASA Wind Product (i.e., the Alongshore Wind Stress, AWS; and the Wind Stress Curl, WSC) and From Dynamical Simulations of the Region (i.e., Velocity Based Transport, VBT)

(a)

		DO at 20 m				T at 20 m			
Index	Season	Slope	R	R^2	p-value	Slope	R	R^2	p-value
Alongshore Wind Stress (AWS)	All	−1986.37	−0.683	0.47	<0.01	−35.75	−0.629	0.40	<0.01
	Spring	−2800.46	−0.747	0.56	<0.01	−41.36	−0.628	0.39	<0.01
	Summer	−2003	−0.481	0.23	<0.01	−52.2	−0.399	0.16	<0.01
	Autumn	−2195.34	−0.725	0.53	<0.01	−36.01	−0.647	0.42	<0.01
	Winter	−968.72	−0.498	0.25	<0.01	−18.49	−0.415	0.17	<0.01
Velocity Based Transport (VBT)	All	−958.01	−0.508	0.26	<0.01	−18.75	−0.509	0.26	<0.01
	Spring	−1067.31	−0.621	0.39	<0.01	−16.59	−0.550	0.30	<0.01
	Summer	−539.22	−0.533	0.28	<0.01	−16.31	−0.514	0.26	<0.01
	Autumn	−1168.69	−0.549	0.30	<0.01	−19.59	−0.501	0.25	<0.01
	Winter	−376.12	−0.200	0.04	<0.01	−5.47	−0.127	0.02	0.04
Wind Stress Curl (WSC)	All	27159894	0.684	0.47	<0.01	495,410	0.638	0.41	<0.01
	Spring	32025010	0.689	0.47	<0.01	501,610	0.615	0.38	<0.01
	Summer	14705278	0.345	0.12	<0.01	418,485	0.313	0.10	<0.01
	Autumn	30986475	0.693	0.48	<0.01	528,537	0.644	0.41	<0.01
	Winter	16835229	0.493	0.24	<0.01	316,606	0.405	0.16	<0.01
Temperature (T)	All	34.68	0.816	0.67	<0.01				
	Spring	46.31	0.853	0.73	<0.01				
	Summer	23.4	0.884	0.78	<0.01				
	Autumn	40.24	0.904	0.82	<0.01				
	Winter	17.4	0.412	0.17	<0.01				

(b)

			DO				Observed T			
Location	Index	Season	Slope	R	R^2	p-value	Slope	R	R^2	p-value
70 m	AWS	All	−407.2	−0.191	0.04	<0.01	−15.98	−0.616	0.38	<0.01
		Spring	242.98	0.164	0.03	0.33	−29.92	−0.711	0.51	<0.01
		Summer	775.79	0.708	0.5	<0.01	−5.41	−0.603	0.36	0.01
		Autumn	−221.9	−0.428	0.18	<0.01	−5.58	−0.729	0.53	<0.01
		Winter	−868.2	−0.4	0.16	<0.01	−7.34	−0.35	0.12	<0.01
	VBT	All	83.74	0.047	0	0.51	−12.18	−0.568	0.32	<0.01
		Spring	205.46	0.24	0.06	0.15	−15.02	−0.618	0.38	<0.01
		Summer	537.67	0.728	0.53	<0.01	−3.69	−0.609	0.37	<0.01
		Autumn	−26.74	−0.144	0.02	0.25	−1.64	−0.597	0.36	<0.01
		Winter	−1103	−0.306	0.09	<0.01	−10.29	−0.295	0.09	0.01
	WSC	All	−463579.11	−0.014	0	0.85	256398	0.638	0.41	<0.01
		Spring	−5232627	−0.282	0.08	0.09	380648	0.723	0.52	<0.01
		Summer	−5437458	−0.373	0.14	0.14	57401	0.481	0.23	0.05
		Autumn	1866744	0.386	0.15	<0.01	48414	0.679	0.46	<0.01
		Winter	9548569	0.163	0.03	0.17	89432	0.158	0.02	0.19

Table 3
Continued

(b)

Location	Index	Season	DO Slope	DO R	DO R^2	DO p-value	Observed T Slope	Observed T R	Observed T R^2	Observed T p-value
	Model T	All	29.7	0.36	0.13	<0.01				
		Spring	13.5	0.38	0.14	0.02				
		Summer	−114.3	−0.94	0.88	<0.01				
		Autumn	16.7	0.25	0.06	0.05				
		Winter	101.7	0.98	0.96	<0.01				

Note. Calculations are based on 7-day, rolling averages of the variables. The standard errors were ≤0.02 for all variables tested.

T (to 15°C) coincident with reversals in the AWS and the WSC (net Ekman convergence), as well as net downward vertical transport apparent from the VBT. One such downwelling event for which we have coincident records of T and DO features prominently in the summer of 2009.

Hypoxic conditions recorded at the 20 m mooring were rapidly ventilated during seasonal transitions between wind states in autumn and early winter. Upwelling metrics (AWS and WSC) consistently explained less of the variance in DO and T during winter than during the upwelling season (Table 3). Nevertheless, well-ventilated waters were associated with downwelling-favorable AWS and a positive (convergent) WSC, and generally associated with negative VBT, indicative of downwelling. Sporadic excursions to upwelling favorable conditions coincided with rapid declines in DO. Specifically, during the winters of 2009, 2010, and 2011, DO concentrations at 20 m declined to ≤60 μmol kg^{-1} during upwelling favorable conditions (Figure 5).

3.3. On-Shelf Modification of Nitrate and Oxygen Tracers

3.3.1. Mid-Bay

Positive ΔNO_3^- and ΔAOU below the surface in the mid-bay region provide evidence for nutrient trapping year-round (Figure 7). Instances of negative ΔAOU and/or ΔNO_3^- expectedly corresponded to shallow depths (generally <25 m), consistent with the photosynthetic drawdown of nutrients and net oxygen production. Nitrate loss to denitrification was also evident in all seasons, most notably in summer, autumn, and winter, as indicated by data below the Redfield ratio line (Figure 7).

Quantifying ΔNO_3^- and ΔAOU using the SHBML climatology of de Villiers (2017) similarly reveals evidence of nutrient trapping in the subsurface year-round. The most sustained nutrient trapping occurs in the mid-bay region and the most severe following the upwelling season in May, at which time ΔAOU and ΔNO_3^- are the highest (Figure 8). The weakest nutrient trapping signal is evident during the spring (Figures 8e and 8f) when flushing by offshore waters likely resets the physicochemical conditions of the shelf. In contrast to the nearshore, where ΔAOU and ΔNO_3^- not only decline but even change sign in autumn, climatological ΔAOU and ΔNO_3^- remain elevated in the mid-bay region year-round (Figures 8 and 9).

3.3.2. Nearshore

Inshore of the 50 m isobath, the water column AOU and N concentrations revealed seasonal differences in the relative influence of various overlapping physical and biogeochemical processes (Figure 10; Table 3). Beneath the surface (i.e., for data from deeper than 5 m) in spring and summer, ΔAOU and ΔNO_3^- were generally positive, indicating the depletion of DO and the accrual of nitrate from remineralization (i.e., nutrient trapping; Flynn et al., 2020). In both seasons, however, most of the subsurface ΔNO_3^- values fell below the expected (i.e., Redfieldian) relationship with ΔAOU, suggestive of coincident N loss from denitrification. In the subsurface in autumn, ΔNO_3^- was generally negative at positive ΔAOU (Table 3), indicating N loss to denitrification, which likely occurred mainly in the sediments. It is worth noting that ΔAOU was significantly modified relative to the source waters at all times of year (Table 4), whereas ΔNO_3^- was only different in the spring and autumn (Table 4). In Figure 10, ΔNO_3^- appears modified in summer as most of the observations reside outside the center

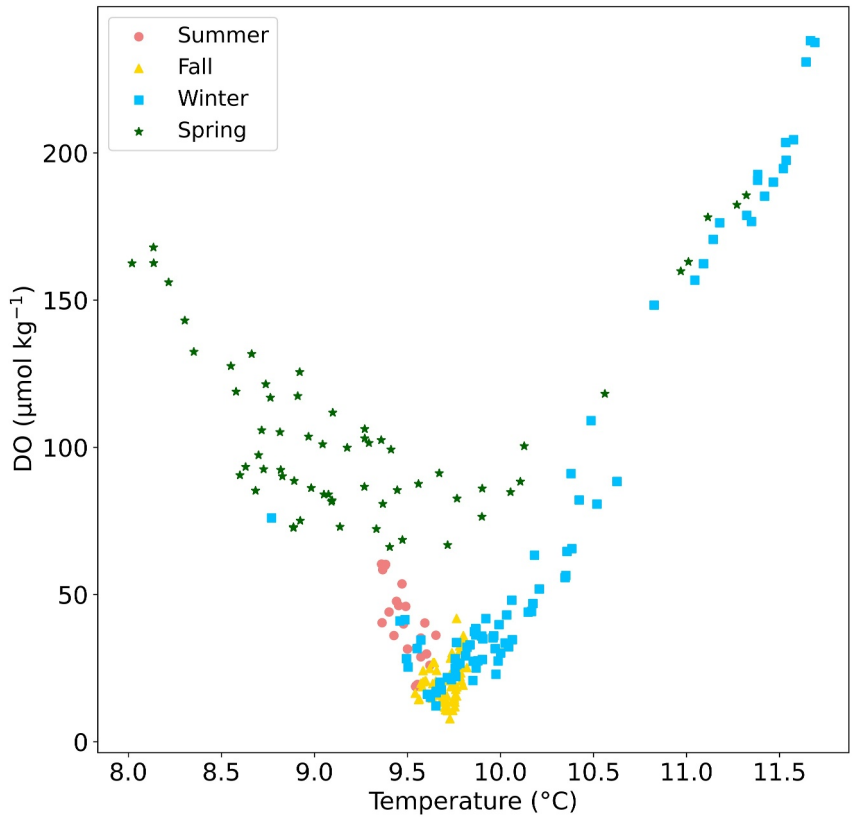

Figure 6. Scatter plot of DO concentration (µmol kg^{-1}) relative to T (°C) from the 70 m mooring spanning February–November 2012 (Pitcher et al., 2014) with the color bar indicating the month of the observations. Seasonal groupings are: spring (September, October, and November), summer (February), autumn (March, April, and May), and winter (June, July, and August).

square of uncertainty associated with the MLR, but this modification was not found to be statistically significant. All these analyses indicate that even source waters delivered to nearshore at the onset of the upwelling season were shelf-modified and likely originated on-shelf from the mid-bay.

During winter, by contrast, we observed almost no incidence of positive ΔAOU. Instead, much of the data signaled increased ventilation relative to the source waters (e.g., negative ΔAOU, median value = −60 µmol kg^{-1}), implicating a deep wind-mixed surface layer and/or net photosynthetic O_2 production. These data are consistent with the higher DO concentrations observed in winter at the 20 m mooring (Figure 5). The coincident wintertime nitrate concentrations were coherently more depleted than in source waters (negative ΔNO_3^-, median = −4.1 µmol kg^{-1}), indicating net photosynthetic assimilation of nitrate by phytoplankton. A similar signal was also apparent in autumn, predominantly in the upper ∼5–10 m, although with ΔAOU that was always higher than in winter. The implication is that ventilation was far weaker in autumn than in winter.

We additionally used the SHBML climatology of de Villiers (2017) to quantify the ΔNO_3^- and ΔAOU across the shelf. This exercise reveals that on average, the magnitude and extent of nearshore nutrient trapping varies seasonally (Figure 8). Subsurface ΔAOU reaches a maximum in the autumn (May), but unlike in summer (February) and spring (September), is accompanied by a negative ΔNO_3^- at this time (Table 4), which, consistent with the nearshore quadrant plot (Figure 10), indicates that N loss to denitrification was strongest at the end of upwelling season.

4. Discussion

Developing a mechanistic understanding of the drivers of hypoxia is necessary to support predictions. To this end, we collated and analyzed 25 years of in situ DO and hydrographic observations in relation to a high-resolution

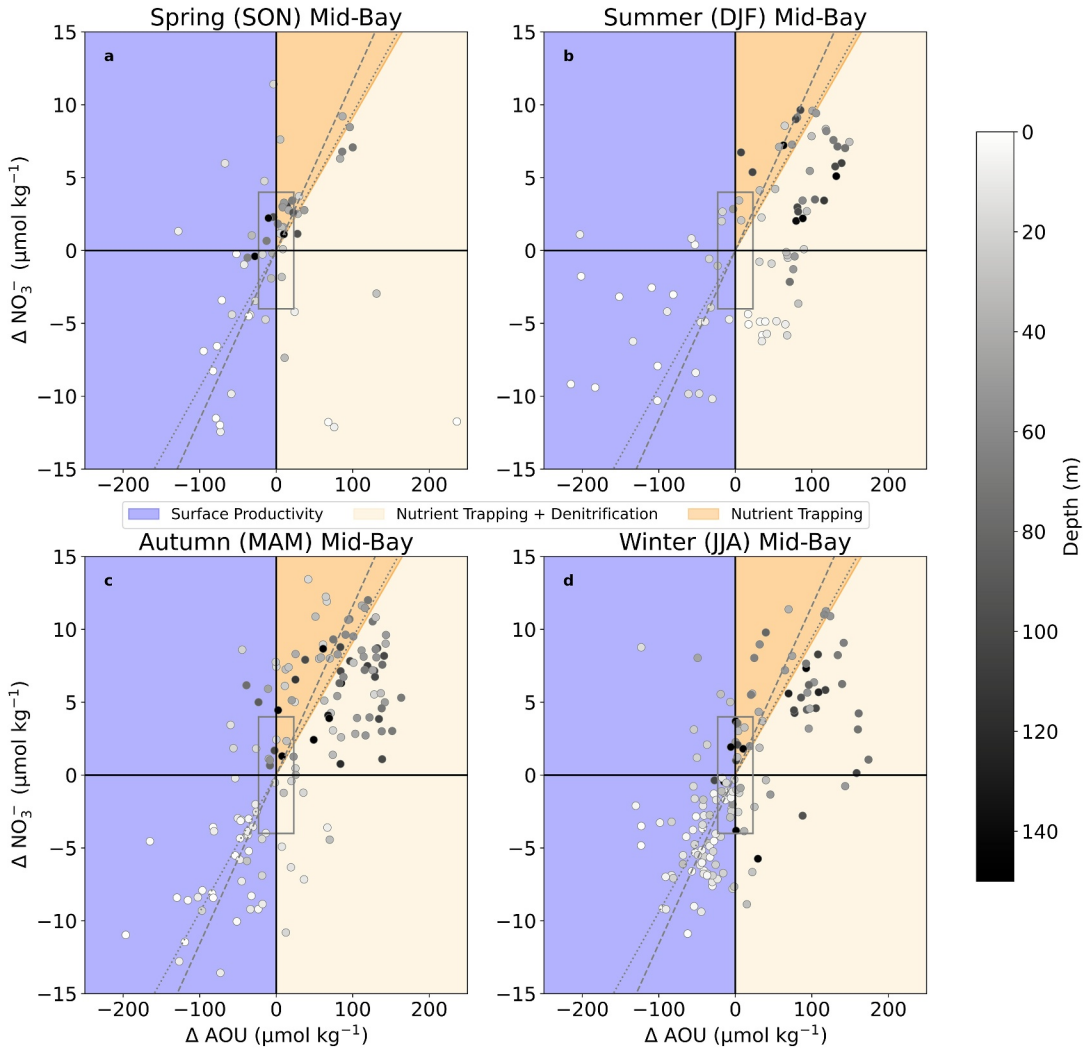

Figure 7. ΔNO_3^- versus ΔAOU for the mid-bay stations (SHBML 3, 4, 5 and 22) situated between the 50 and 150 m isobaths in (a) spring, (b) summer, (c) autumn, and (d) winter. Error associated with the MLRs is indicated by the gray box around the origin; data points falling outside of this box indicate on-shelf modification of source waters. The gray lines show the expected nitrate concentration for a given AOU if remineralization occurs at a constant Redfield ratio (dashed line = $16NO_3^-$:138AOU; dotted line = $16NO_3^-$:170AOU). Please see Figure S2 in Supporting Information S1 for a visual representation. Observation counts are: spring (58), summer (81), autumn (141), and winter (140).

model output from the SHB region of the SBUS. We developed new metrics that rely on a statistical model extending basic local hydrographic observations to N and DO. We found significant relationships between subsurface DO and the magnitude of wind-based upwelling, which varied with season and region within SHB. From the new statistical metrics, we identify periods when nutrients accumulate on the shelf in excess of those present in upwelled source waters. These relationships reveal potential mechanisms for the seasonal decline of DO and suggest that source water provenance changes as the upwelling season progresses. Possible drivers of this change are explored below.

4.1. Oxygen Dynamics in St Helena Bay During the Upwelling Season

Dissolved oxygen concentrations in the nearshore decreased in response to upwelling-favorable wind events. The water that supplies this region was low in oxygen year-round, reaching a minimum in autumn. Normoxic conditions were restored during downwelling events following the relaxation of upwelling-favorable winds. In all, DO concentrations in the nearshore region of SHB proved highly responsive to incident winds.

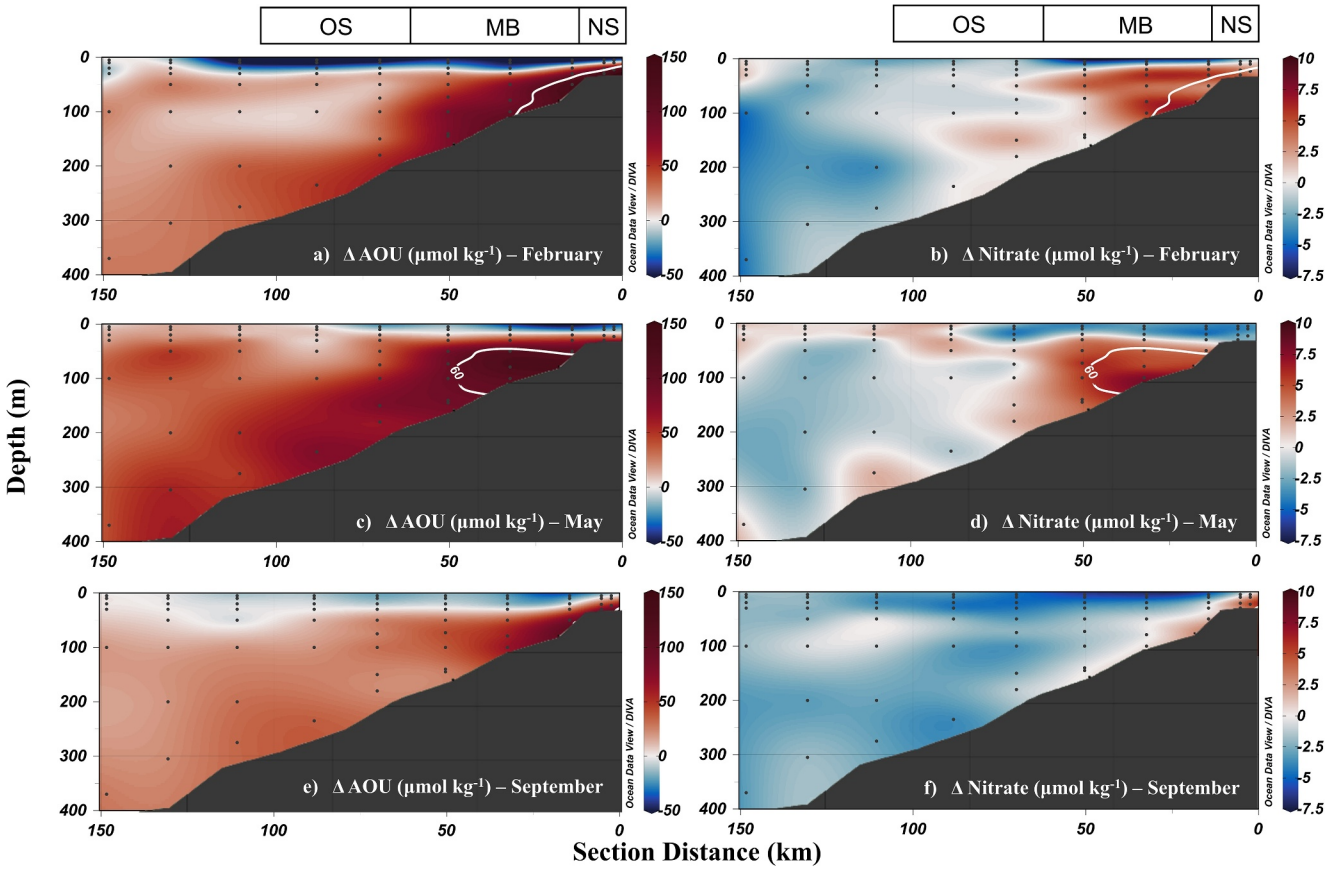

Figure 8. Cross-sections showing ΔAOU (a, c, and e; left panels) and ΔNO_3^- (b, d, and f; right panels) calculated from the SHBML climatology (de Villiers, 2017) for (a)–(b) February (c)–(d) May, and (e)–(f) September. Discrete sampling depths are indicated by the black dots, the hypoxia threshold of 60 µmol kg^{-1} is indicated by the white contour line; where this contour is not visible, the hypoxia threshold was not reached. The regions of the shelf are denoted by the bar above the top panels (NS = nearshore, MB = mid-bay, and OS = outer-shelf). MLRs used to calculate ΔAOU and ΔNO_3^- are associated with an uncertainty of ±23 and ±4 µmol kg^{-1}, respectively.

In contrast to the nearshore, where hypoxic waters coincided with upwelling events, subsurface hypoxia was more persistent at 70 m in the mid-bay, consistent with previous observations (Jarre et al., 2015; Pitcher et al., 2014). As documented by Lamont et al. (2018) and borne out by our analysis, oxygenated water replenishes the mid-bay at the onset of upwelling in spring, after which DO declines throughout the upwelling season to reach a minimum in autumn. Ventilation events at the 70 m mooring were relatively modest in summer, associated with both upwelling-favorable winds that supplied colder oxygenated water onshore, as well as with wind relaxations that supplied warmer oxygenated waters, presumably from shallower depths. It is worth noting that Lucas et al. (2014) also observed downwelling of warm surface water in SHB during summer, which influenced water properties down to the bottom of the 50 m water column. In autumn, upwelling-favorable winds were, paradoxically, associated with *decreases* in subsurface DO; the waters replenishing this region, while colder, became lower in oxygen than during spring. The biggest ventilation events occurred in winter, as documented by Pitcher and Probyn (2017) and Pitcher et al. (2023), in association with downwelling and/or deep wind-driven mixing. However, the seasonal maximum MLD was persistently shallower than the depth of the shelf (~50 m, Russo et al., 2022) resulting in portions of the shelf remaining unventilated from one season to the next.

The seasonal differences in the relationship of subsurface DO to alongshore winds highlight a perplexing feature of SHB—namely, the rapid emergence and persistence of hypoxic conditions mid-bay following the oxygenation at the onset of upwelling in spring (Flynn et al., 2020; Pitcher et al., 2014). Because upwelling-favorable winds drive cold oxygenated waters onshore, the negative relationship between DO and upwelling-favorable ASW in autumn is hard to reconcile. The weaker positive slope between DO and upwelling-favorable ASW in summer compared to spring is also puzzling. From the oxygen record at the 70 m mooring (Figures 4 and 6), Pitcher

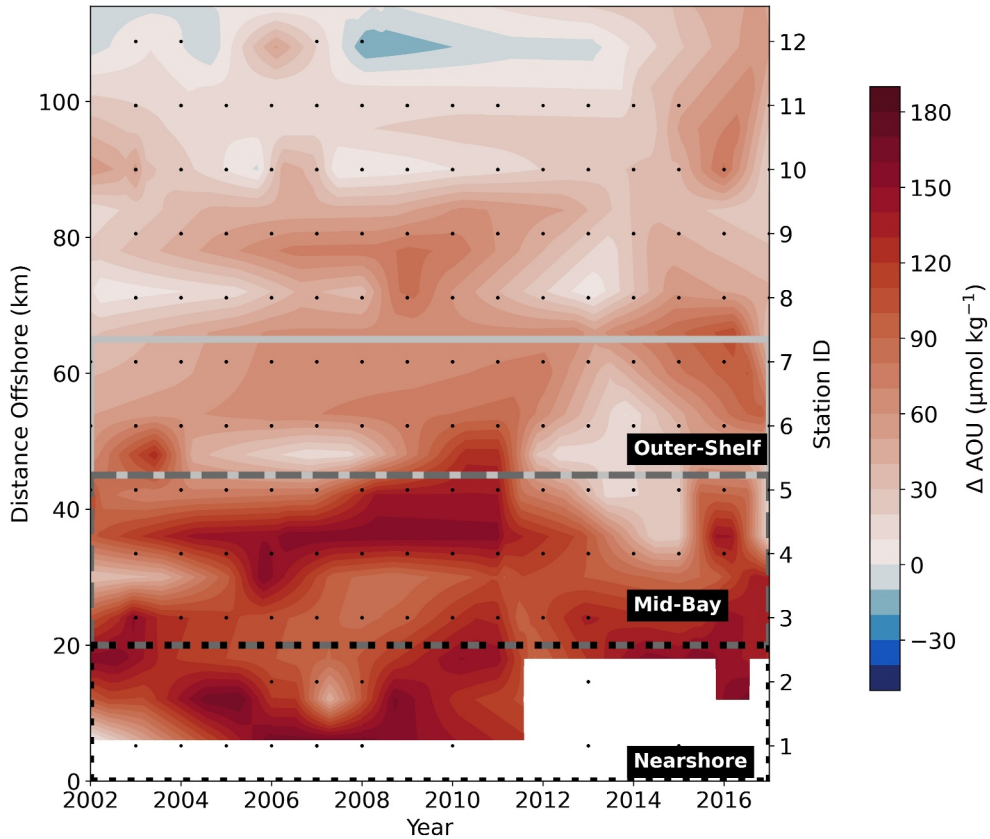

Figure 9. Hovmöller plot showing bottom-depth ΔAOU values from the SHBML between 2002 and 2016. The nearshore region is between the dotted lines, the mid-bay between the dashed lines, and the outer-shelf is the region beyond the solid line. The gray dots indicate discrete measurements.

et al. (2014) similarly noted the changes in seasonal trends between T and DO, as well as the progressive decline of DO over the upwelling season and the coincident increase in T. The authors suggested that these dynamics can be explained by a seasonal decrease in wind intensity, whereby a progressively lower quantity of cold oxygenated water is entrained onshore as the upwelling season proceeds. The high-resolution wind product used to drive the model simulations explored here allows us to evaluate this idea: Mean upwelling winds from 2008 to 2012 (Table 2) were of similar amplitude during the spring and summer months, and only slightly lower in autumn. These metrics are somewhat biased, however, as they include days succeeding the end of the upwelling season. Regardless, upwelling-favorable winds in summer were not reduced relative to spring. We thus conclude that a progressive decrease in wind strength does not satisfactorily explain the trends we observed and described by Pitcher et al. (2014).

We instead hypothesize that the composition of the source waters replenishing SHB changes over the course of the upwelling season, and/or that the provenance of the source waters changes, such that waters upwelled into the bay are lower in DO and higher in T later in the season (Figure 11). For a given upwelling metric, the respective correlations to temperature were considerably stronger in spring than in summer and autumn, suggesting that the upwelled water that replenishes the shelf, while colder than on-shelf waters, is not as cold in summer and autumn as during the onset of the upwelling season in spring. By itself, the higher T of the source water in summer and autumn suggests that it originated from a shallower offshore trajectory, or that it had a more nearshore origin. The lower DO signature in autumn, in turn, argues specifically for a more nearshore provenance, wherein water that was more "aged" in the nearshore would incur enhanced and relevant changes in biogeochemical properties from remineralization.

The seasonal evolution of biogeochemical properties in the subsurface of SHB corroborates the ventilation dynamics inferred above. ΔAOU and ΔNO_3^- were most similar to the offshore source waters in spring, signaling

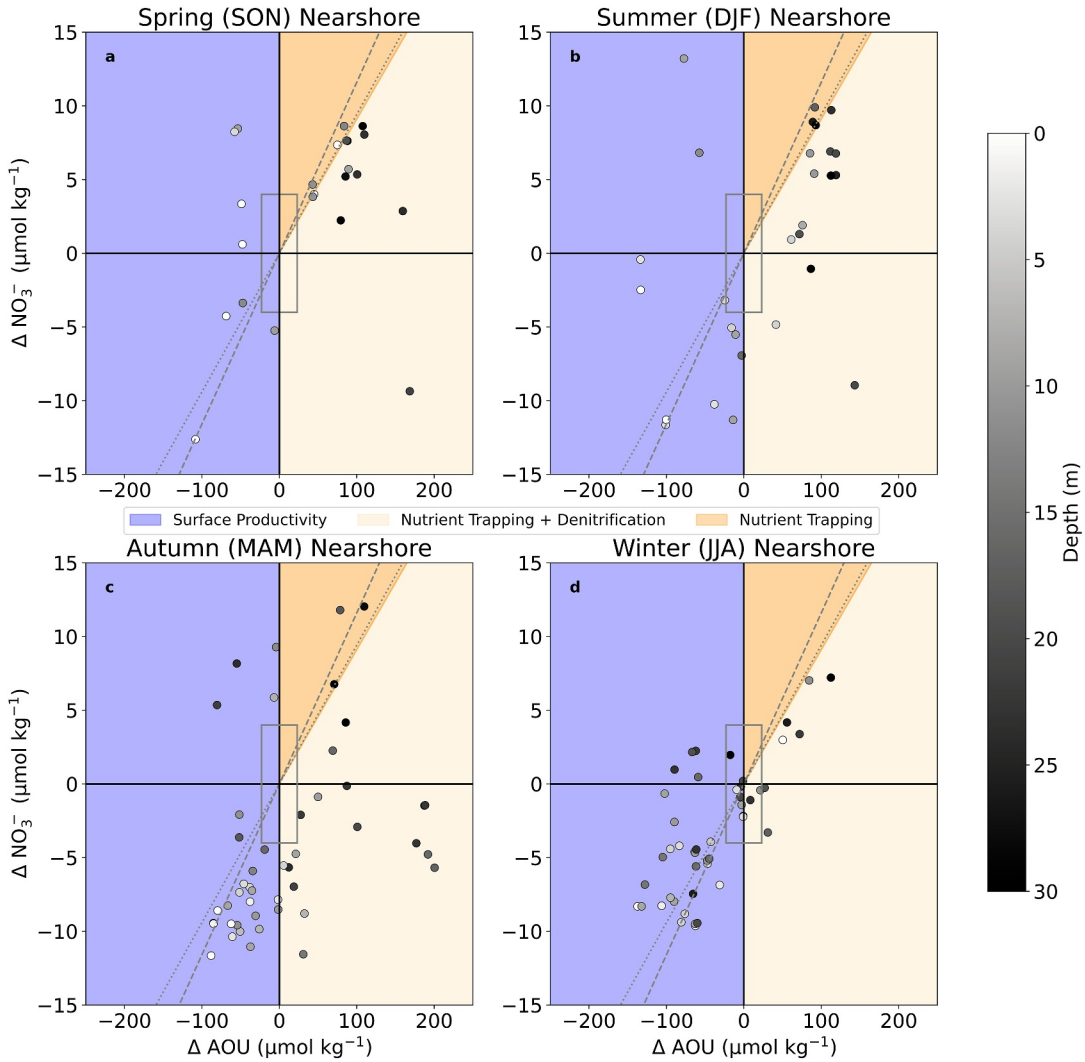

Figure 10. Nearshore (≤50 m bottom depth) ΔNO_3^- versus ΔAOU for (a) spring, (b) summer, (c) autumn, and (d) winter. Error associated with the MLRs is indicated by the gray box around the origin; data points falling outside of this box indicate on-shelf modification of source waters. The gray lines show the expected nitrate concentration for a given AOU if remineralization occurs at a constant Redfield ratio (dashed line = $16NO_3^-$:138AOU; dotted line = $16NO_3^-$:170AOU). Please see Figure S2 in Supporting Information S1 for a visual representation. Observation counts are: spring (23), summer (28), autumn (47), and winter (47). The colors of the symbols indicate the water column depth where the sample was taken.

the entrainment of oxygenated SAMW onto the shelf at the onset of upwelling. ΔAOU and ΔNO_3^- increased at the subsurface throughout the upwelling season with N loss to denitrification becoming evident in autumn when DO was correspondingly lowest. Flynn et al. (2020) hypothesized that the accrual of remineralized products inshore (nutrient trapping) throughout the broader SBUS arises in part from the retentiveness of inshore waters, promoted by the development of the equatorward Columbine jet and its associated front during the upwelling season. Repeated cycles of upwelling and remineralization result in a progressively larger nutrient reservoir at depth that is subsequently upwelled to the surface, fueling progressively larger phytoplankton blooms that are remineralized at the subsurface, steadily depleting DO (increasing ΔAOU) as the season advances. The depletion of DO, in turn, fosters progressively more denitrification, largely benthic, although occasionally occurring in the water column - evidenced from the apparent N deficit in autumn (Flynn et al., 2020; Pitcher & Probyn, 2017; Tyrell & Lucas, 2002). Denitrification thus provides a negative feedback to shelf productivity. The retention invoked by Flynn et al. (2020) to explain the substantial accrual of nutrients and ΔAOU inshore is consistent with the change of provenance of upwelled waters postulated here, from offshore in spring to nearshore in summer and

Table 4
Seasonal Descriptive Statistics for ΔNO_3^- and ΔAOU by Region

Location	Parameter	Season	Min	Max	Median	Average	Observation # (n)
Nearshore	Delta NO3	Spring	−12.62	8.63	**4.67**	2.94	23
		Summer	−11.64	13.21	1.11	0.53	28
		Autumn	−11.65	12.03	**−5.68**	−3.97	47
		Winter	−9.63	7.21	−3.93	−3.06	47
	Delta AOU	Spring	−108.26	168.53	**74.97**	**40.32**	23
		Summer	−133.47	143.23	**66.56**	**28.46**	28
		Autumn	−88.08	200.59	−6.81	10.75	47
		Winter	−137.35	112.46	**−60.00**	**−40.18**	47
Mid-Bay	Delta NO3	Spring	−12.44	11.40	0.85	−0.61	58
		Summer	−10.31	9.64	0.39	0.43	81
		Autumn	−13.57	13.43	3.06	2.00	141
		Winter	−10.88	11.37	−1.25	−0.51	140
	Delta AOU	Spring	−127.92	236.23	3.56	0.70	58
		Summer	−214.81	149.07	**47.44**	**24.55**	81
		Autumn	−196.53	163.40	**25.31**	**30.78**	141
		Winter	−130.06	174.07	−6.20	4.03	140
Outershelf	Delta NO3	Spring	−12.25	4.59	−0.26	−1.17	47
		Summer	−12.86	5.22	−0.78	−1.07	63
		Autumn	−7.83	13.00	0.26	0.61	84
		Winter	−6.08	10.37	−1.58	−1.01	90
	Delta AOU	Spring	−60.80	64.55	−21.05	−17.62	47
		Summer	−158.84	68.78	−3.20	−9.15	63
		Autumn	−127.70	88.76	−7.20	−7.18	84
		Winter	−123.34	53.30	−13.68	−11.42	90

Note. Bold font indicates median values outside the range of uncertainty of the MLR, which are therefore considered significantly modified.

autumn. The ΔAOU signal that accrued over the upwelling season in the nearshore potentially explains why upwelling in autumn was associated with replenishment by colder yet less oxygenated water at 70 m in SHB.

We emphasize that subsurface respiration undoubtedly ramps up following the onset of upwelling, a dynamic that could arguably account for the persistence and seasonal intensification of subsurface hypoxia in SHB. Although undeniably contributing to hypoxia, subsurface respiration and its seasonal intensification do not, however, account for the weaker subsurface supply of cold water for a given upwelling intensity in summer and autumn, nor for the decrease in subsurface DO directly associated with upwelling events in autumn. Oxygen dynamics in SHB and in the inshore region of the broader SBUS evidently involve an intricate interplay between physical and biogeochemical dynamics.

Our contention that the provenance of the shelf waters changes over the upwelling season, becoming more shelf-aged, has precedent in other upwelling regions. In the northern California current system (n-CCS), the provenance of upwelling source waters has been shown to shoal during the upwelling season (He & Mahadevan, 2021; Jacox & Edwards, 2011; Lentz & Chapman, 2004; McCabe et al., 2015). At a mid-shelf location, a subsurface onshore return layer develops midseason, with the timing thereof coinciding with the changing direction of the alongshore sea level gradient. In addition, a third layer develops near the shelf bottom and flows offshore. This circulation likely has implications for oxygen and shelf biogeochemical cycles in the n-CCS system as well.

Salient differences between the n-CCS and the SBUS could contribute to differences between the dynamics described by McCabe et al. (2015) and those in the SHB, particularly shelf width and freshwater delivery, with the SBUS experiencing very little of the latter. Although the n-CCS has a wide shelf for the CCS region, it is

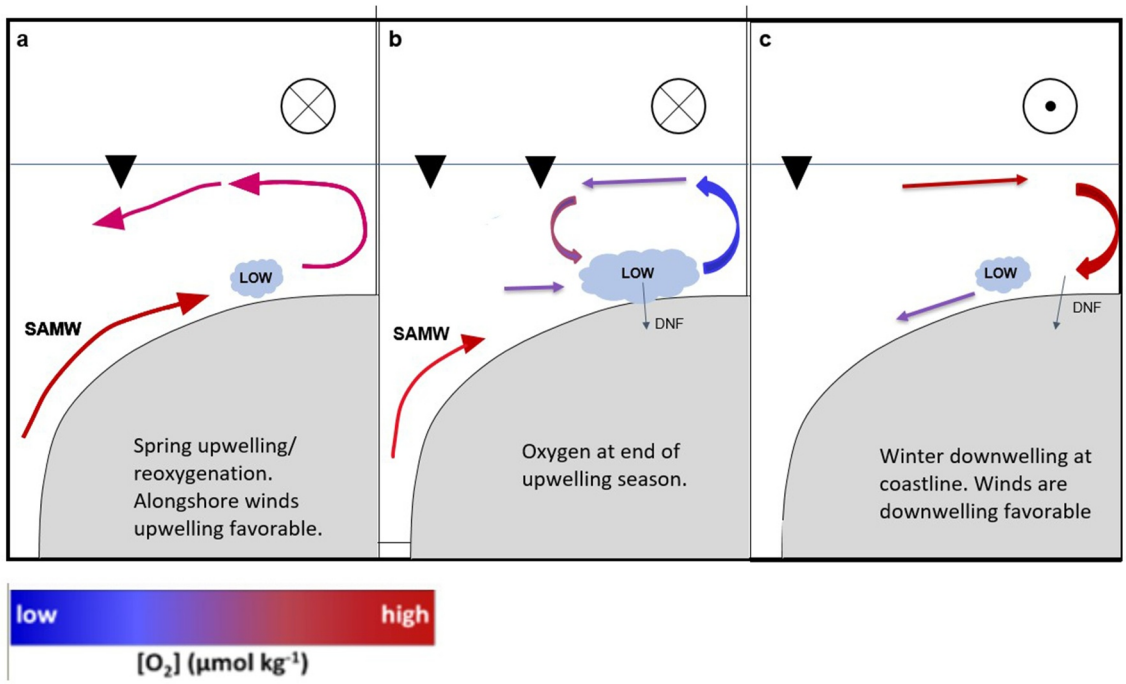

Figure 11. Upwelling case and generalized SHB dynamics in cross-section over three seasons: (a) spring/early summer, (b) late summer/autumn, (c) winter. The updated nutrient trapping hypothesis where the circulation is depicted with colors corresponding to the degree of relative oxygenation; red is the most oxygenated and blue the least. The fronts are indicated by the triangles at the surface, with wind direction and magnitude depicted by the jets in the atmosphere. Denitrification (DNF) is depicted with arrows into the sediments. The upwelling SAMW source water is also shown.

substantially narrower than the SBUS shelf. Monteiro et al. (2011) proposed that the width of the shelf is a strong predictor of the likelihood of hypoxia as the offshore export of organic material is greatly reduced in wide-shelf systems, so more organic material is respired at the shelf bottom. Others have also identified shelf width as potentially playing an important role in off-shelf export of material and as being associated with recirculation or retention (Hickey & Banas, 2008; Liu et al., 2019; Schmidt & Eggert, 2016; Sharples et al., 2017). If the return flow in the SBUS shoals over the upwelling season as in the n-CCS (McCabe et al., 2015), then the width of the shelf would exacerbate this retention dynamic. A shallower return flow would disrupt offshore export pathways for organic material at the subsurface in response to downwelling or relaxation events, encouraging retention of organic material on the shelf. The presence of the fronts in the SBUS may further alter the offshore export of organic material, isolating the mid-bay waters from potential ventilation.

4.2. The Re-Occurrence of Mid-Bay Hypoxia During Winter

The observations presented here in relation to prior analyses (Flynn et al., 2020; Pitcher et al., 2014; Pitcher & Probyn, 2017) and existing climatologies (de Villiers, 2017) reveal that hypoxia persists in the mid-bay of SHB in winter. As noted by others (Pitcher et al., 2014; Pitcher & Probyn, 2017), the incidence of hypoxia in winter is counterintuitive, given lower incident primary production, weaker stratification, and, as revealed in this study, stronger and more persistent downwelling favorable winds. Although periods of downwelling in the SBUS are not well documented in the literature, downwelling winds were associated with the largest ventilation events in the observational records likely driven by winter storms, yet provided intermittent relief from local hypoxia at 70 m, as hypoxic waters appeared to re-invade following relaxations. This dynamic invokes a see-saw mechanism whereby water sloshes back and forth in SHB in winter but is not replenished by onshore flows of oxygenated water nor by wind mixing events that reach bottom depths.

The lack of prolonged ventilation to reoxygenate the entire water column or region of the SHB subsurface explains why the biogeochemical properties, ΔAOU, ΔNO_3^-, and N deficit, remained relatively high mid-bay in winter. From analogous observations for the whole of the SBUS made during one winter season, Flynn

et al. (2020) hypothesized that subsurface properties remain highly modified relative to off-shelf waters despite the lower surface productivity because of a longer residence of water on the shelf in winter compared to the upwelling season, consistent with our multi-year analysis. At the onset of upwelling following winter, the pool of low oxygen water in the mid-bay subsurface is available to re-upwell in the nearshore. The potential limiters to the seemingly never-ending positive loop set up by nutrient trapping on the shelf include the degree of ventilation and the amount of denitrification. The magnitude and relative importance of these two negative feedbacks could control the severity of hypoxia in this region.

4.3. Connectivity/Source Waters to the Nearshore

The chemical properties in the nearshore are influenced by the subsurface waters from which they derive. Nutrient trapping was repeatedly identified in the nearshore in spring through the coincidence of positive ΔNO_3^- and ΔAOU, which also indicate on-shelf modification of the source waters (Table 4). Even in the spring, when the upwelling of offshore water flushed the shelf, the nearshore upwelling shelf-modified water likely originated from the mid-bay region. In autumn, the nearshore subsurface was characterized by positive ΔAOU but negative ΔNO_3^-, indicating significant denitrification. As per the hypotheses of Flynn et al. (2020), nutrients trapped in the mid-bay region could be supplied to the surface during the following upwelling seasons, fueling phytoplankton blooms and exacerbating local oxygen drawdown; however, the nitrogen may not be available if denitrification removes a significant quantity from the system. The modified signal contains the accrual of AOU and other respiration products caused by nutrient trapping inshore (Flynn et al., 2020), potentially related to altered circulation patterns associated with fronts and seasonal changes in upwelling patterns, regardless, the modification signal appears to persist interannually.

In summer to early autumn, hypoxic events in the nearshore corresponded to the upwelling of colder but modified, or shelf-aged (i.e., low DO) source waters. The immediate provenance of this water is likely the mid-bay or lateral transport from the north of the shelf (Fawcett et al., 2008; Lucas et al., 2014; Send & Nam, 2012). Grant & Jacinto (2020) describe a mechanism whereby dinoflagellate blooms are concentrated near the coast of the SBUS during wind relaxations or reversals; the development of a poleward counter-current inshore transports these blooms into SHB, supplying exogenous organic material that is respired in the bay. A strong thermocline has been observed in this region in late summer/autumn, separating the well-oxygenated surface waters from the oxygen depleted bottom waters (Hutchings et al., 2012). These observations are all consistent with the seasonal changes in source water provenance that we suggest.

4.4. Implications for Marine Resource Managers and Predicting Lobster Walk Outs

When oxygen levels are severely low, rock lobsters walk out of SBH and onto the shore. The Department of Forestry, Fisheries and the Environment (DFFE) attempts to save them by moving them to more oxygenated waters, yet most perish (DFFE, 2023). Walk outs have been tied to low-oxygen events associated with the accumulation and decay of dense dinoflagellate blooms during the late summer/early autumn (Cockcroft, 2001, 2008; Cockcroft et al., 1999), but the connection between the long-term/decadal deterioration of the lobster fishery and changing ocean conditions such as deoxygenation has yet to be established. Several walk out events have been well characterized and have been shown to coincide with anoxic conditions through the entire shallow inshore water column following the decay of massive red tide blooms: March 2009 event see Pitcher and Probyn (2011); February 2015 event see Ndlovu et al. (2017), Pitcher et al. (2021); March 2022 event see Pitcher et al. (2023). Lobsters seem unable to seek refuge and are likely boxed in by habitat compression driven by hypoxic waters offshore that force them out of the water and onto the beach. For the nearshore region of SHB (<20 m deep), we find a significant relationship between the AWS and DO concentrations which suggests that low oxygen events in this nearshore zone could be predicted from the winds if the wind data were available in real time. This may add some prediction capabilities to the walk outs themselves as the cold, low oxygen water that upwells nearshore, and that this study is able to predict, causes habitat compression. The upwelling of this water, particularly during autumn when oxygen is very low, causes rock lobsters to aggregate in high numbers in shallow waters (<10 m). Here they are vulnerable to events of anoxia following the decay of high biomass red tides. Under quiescent conditions, these blooms accumulate inshore in warm waters, eventually die-off causing anoxic conditions that lead to the mortality of the inshore congregations of lobster. HABs have been cited as a possible driver of lobster walk outs in the SBUS because of their potential causal relationship with hypoxia (Pitcher et al., 2014). We suggest that monitoring the mid-bay as the source waters for upwelling in the nearshore alongside the local

winds will yield prognostic information for this complicated system. In addition, additional moored observations of summer conditions are needed to better balance the frequency of observations year-round. However, numerous questions remain such as why the mid-bay pool of low oxygen water expands mid-season, why it only occasionally ventilates, and why spring delivery of off-shelf source water is cut off midway through the season.

Conflict of Interest

The authors declare no conflicts of interest relevant to this study.

Data Availability Statement

Tables S2 and S3 in Supporting Information S1 in the supplemental data file. IEP (Integrated Ecosystem Program) data are available on the MIMS (Marine Information Management System) website: https://data.ocean.gov.za/mims/catalog/?q=iep&sort=rank+desc where each cruise has its own DOI. Some examples used here include (DOI: 10.15493/dea.mims.26052243, DOI: 10.15493/dea.mims.26052250, DOI: 10.15493/dea.mims.26052251, DOI: 10.15493/dea.mims.26052245). The data from SADCO (Southern African Data Centre for Oceanography) are available here: http://sadco.ocean.gov.za/. CLIVAR data are available on the CCHDO (CLIVAR and Carbon Hydrographic Data Office) website: https://cchdo.ucsd.edu/. The CROCO configuration files used to generate the model output analyzed in this study are available via the following DOI: https://doi.org/10.5281/zenodo.7947550. A compilation of the raw data supporting the conclusions of this article will be made available by the authors upon request, without undue reservation. The figures were generated using Python and Ocean Data Viewer.

Acknowledgments
We would like to thank DFFE for sharing their oxygen and temperature data as well as their expertise. AJC, SAS, MZ, and JG were supported by the US National Science Foundation (OCE-1924270) and RFF and SEF received support from the South African National Research Foundation (129320). We would like to acknowledge Jessica Burger, Keshnee Pillay, Raymond Roman, and Sina Wallschuss for their help collecting and analyzing the nutrient data.

References

Akaike, H. (2011). Akaike's information criterion. In M. Lovric (Ed.), *International encyclopedia of statistical science*. Springer. https://doi.org/10.1007/978-3-642-04898-2_110

Bailey, G. W. (1987). Distribution and cycling of nutrients at four sites in the Benguela system. In C. Bas, R. Margalef, & P. Rubles (Eds.), *International symposium on most important upwelling areas off western Africa (Cape Blanco and Benguela)* (pp. 305–317). Instituto de Investigaciones Pesqueras.

Bailey, G. W. (1991). Organic carbon flux and development of oxygen deficiency on the modern Benguela continental shelf south of 22S: Spatial and temporal variability. In R. V. Tyson & T. H. Pearson (Eds.), *Modern and ancient continental shelf anoxia* (pp. 171–183). Geol. Soc., London.

Bailey, G. W., & Chapman, P. (1985). The nutrient status of the st Helena bay region in february 1979. In L. V. Shannon (Ed.), *South African Ocean Colour and upwelling experiment* (pp. 125–145). Sea Fisheries Research Institute.

Bailey, G. W., & Chapman, P. (1991). Short-term variability during an anchor station study in the southern Benguela upwelling system: Chemical and physical oceanography. *Progress in Oceanography*, *28*(28), 9–37. https://doi.org/10.1016/0079-6611(91)90019-i

Breitburg, D., Levin, L. A., Oschlies, A., Grégoire, M., Chavez, F. P., Conley, D. J., et al. (2018). Declining oxygen in the global ocean and coastal waters. *Science*, *359*(6371), eaam7240. PMID: 29301986. https://doi.org/10.1126/science.aam7240

Burger, J. M., Moloney, C. L., Walker, D. R., Parrott, R. G., & Fawcett, S. E. (2020). Drivers of short-term variability in phytoplankton production in an embayment of the southern Benguela upwelling system. *Journal of Marine Systems*, *208*, 103341. https://doi.org/10.1016/j.jmarsys.2020.103341

Calvert, S. E., & Price, N. B. (1971). Upwelling and nutrient regeneration in the Benguela current. *Deep-Sea Research*, *18*(5), 505–523. https://doi.org/10.1016/0011-7471(71)90074-x

Cockcroft, A. C. (2001). Jasus lalandii 'walkouts' or mass strand-ings in South Africa during the 1990s: An overview. *Marine and Freshwater Research*, *52*(8), 1085–1094. https://doi.org/10.1071/mf01100

Cockcroft, A. C., Schoeman, D. S., Pitcher, G. C., Bailey, G. W., & van Zyl, D. L. (1999). A mass stranding, or 'walk-out', of west coast rock lobster, Jasus lalandii, in Elands Bay, South Africa: Causes, results, and implications. In J. C. Von Vaupel Klein & F. R. Schram (Eds.), *The biodiversity crisis and Crustacea* (pp. 673–688). Crustacean Issues12.

Cockcroft, A. C., Van Zyl, D. L., & Hutchings, L. (2008). Large-scale changes in the spatial distribution of South African west coast rock lobsters: An overview. *African Journal of Marine Science*, *30*(1), 149–159. https://doi.org/10.2989/AJMS.2008.30.1.15.465

de Decker, A. H. B. (1970). Notes on an oxygen-depleted subsurface current off the west coast of South Africa. Division of Sea Fisheries Investigational Report No. 84.

Demarcq, H., Barlow, R. G., & Hutchings, L. (2007). Application of a chlorophyll index derived from satellite data to investigate the variability of phytoplankton in the Benguela ecosystem. *African Journal of Marine Science*, *29*(2), 271–282. https://doi.org/10.2989/ajms.2007.29.2.11.194

de Villiers, S. (2017). Biogeochemical climatology for the Southern Benguela Upwelling System, constructed from in situ monthly monitoring data collected from 2001 to 2012. *Department of Environmental Affairs, PANGAEA*. https://doi.org/10.1594/PANGAEA.882218

Diaz, R. J., & Rosenberg, R. (2008). Spreading dead zones and consequences for marine ecosystems. *Science*, *321*(5891), 926–929. https://doi.org/10.1126/science.1156401

Duncombe Rae, C. M. (2005). A demonstration of the hydrographic partition of the Benguela upwelling ecosystem at 2640'S. *African Journal of Marine Science*, *27*(3), 617–628. https://doi.org/10.2989/18142320509504122

Fawcett, A., Pitcher, G. C., & Shillington, F. (2008). Currents of the nearshore region on the southern Namaqua shelf of the southern Benguela. *Continental Shelf Research*, *28*(8), 1026–1039. https://doi.org/10.1016/j.csr.2008.02.005

Fearon, G., Herbette, S., Cambon, G., Veitch, J., Meynecke, J., & Vichi, M. (2023). The land-sea breeze influences the oceanography of the southern Benguela upwelling system at multiple time-scales. *Frontiers in Marine Science*, *10*, 1186069. https://doi.org/10.3389/fmars.2023.1186069

Fearon, G., Herbette, S., Veitch, J., Cambon, G., Lucas, A. J., Lemarié, F., & Vichi, M. (2020). Enhanced vertical mixing in coastal upwelling systems driven by diurnal-inertial resonance: Numerical experiments. *Journal of Geophysical Research: Oceans*, *125*(9), e2020JC016208. https://doi.org/10.1029/2020JC016208

Flynn, R. F., Granger, J., Veitch, J. A., Siedlecki, S., Burger, J. M., Pillay, K., & Fawcett, S. E. (2020). On-shelf nutrient trapping enhances the fertility of the southern Benguela upwelling system. *Journal of Geophysical Research: Oceans*, *125*(6), e2019JC015948. https://doi.org/10.1029/2019JC015948

He, J., & Mahadevan, A. (2021). How the source depth of coastal upwelling relates to stratification and wind. *Journal of Geophysical Research: Oceans*, *126*(12), e2021JC017621. https://doi.org/10.1029/2021JC017621

Hickey, B. M., & Banas, N. S. (2008). Why is the northern end of the California Current System so productive? *Oceanography*, *21*(4), 90–107. https://doi.org/10.5670/oceanog.2008.07

Holden, C. J. (1985). Currents in St Helena Bay inferred from radio-tracked drifters. In L. V. Shannon (Ed.), *South African ocean colour and upwelling experiment*.

Huggett, J., Verheye, H., Escribano, R., & Fairweather, T. (2009). Copepod biomass, size composition and production in the southern Benguela: Spatio-temporal patterns of variation, and comparison with other eastern boundary upwelling systems. *Progress in Oceanography*, *83*(1–4), 197–207. https://doi.org/10.1016/j.pocean.2009.07.048

Hutchings, L., Jarre, A., Lamont, T., van den Berg, M., & Kirkman, S. (2012). St Helena Bay (southern Benguela) then and now: Muted climate signals, large human impact. *African Journal of Marine Science*, *34*(4), 559–583. https://doi.org/10.2989/1814232x.2012.689672

Hutchings, L., Roberts, M. R., & Verheye, H. M. (2009). Marine environmental monitoring programmes in South Africa: A review. *South African Journal of Science*, *105*(3/4), 94–102. https://doi.org/10.4102/sajs.v105i3/4.54

Hutchings, L., van der Lingen, C. D., Shannon, L. J., Crawford, R. J. M., Verheye, H. M. S., Bartholomae, C. H., et al. (2009). The Benguela Current: An ecosystem in four components. *Progress in Oceanography*, *83*(1–4), 15–32. https://doi.org/10.1016/j.pocean.2009.07.046

IOC, SCOR and IAPSO. (2010). *The international thermodynamic equation of seawater – 2010: Calculation and use of thermodynamic properties. Intergovernmental Oceanographic Commission, Manuals and Guides No. 56* (p. 196). UNESCO (English).

Jacox, M. G., & Edwards, C. A. (2011). Effects of stratification and shelf slope on nutrient supply in coastal upwelling regions. *Journal of Geophysical Research*, *116*(C3), C03019. https://doi.org/10.1029/2010JC006547

Jarre, A., Hutchings, L., Crichton, M., Wieland, K., Lamont, T., Blamey, L. K., et al. (2015). Oxygen-depleted bottom waters along the west coast of South Africa, 1950-2011. *Fisheries Oceanography*, *24*(S1), 56–73. https://doi.org/10.1111/fog.12076

Kutner, M., Nachtsheim, C., & Neter, J. (2004). *Applied linear regression models* (4th ed.). McGraw-Hill Irwin.

Laffoley, D., & Baxter, J. M. (2019). *Ocean deoxygenation: Everyone's problem: Causes, impacts, consequences and solutions: Summary for Policy Makers*. International Union for Conservation of Nature (IUCN).

Lamont, T., Hutchings, L., van den Berg, M. A., Goschen, W. S., & Barlow, R. G. (2015). Hydrographic variability in the St. Helena Bay region of the southern Benguela ecosystem. *Journal of Geophysical Research: Oceans*, *120*(4), 2920–2944. https://doi.org/10.1002/2014JC010619

Lamont, T. L., Garcia-Reyes, M., Bograd, S. J., van der Lingen, C. D., & Sydeman, W. J. (2018). Upwelling indices for comparative ecosystem studies: Variability in the Benguela upwelling system. *Journal of Marine Systems*, *188*, 3–16. https://doi.org/10.1016/j.jmarsys.2017.05.007

Largier, J. L. (2020). Upwelling Bays: How coastal upwelling controls circulation, Habitat, and productivity in Bays. *Annual Review of Marine Science*, *12*(1), 415–447. https://doi.org/10.1146/annurev-marine-010419-011020

Lennard, C., Hahmann, A. N., Badger, J., Mortensen, N. G., & Argent, B. (2015). 921 development of a numerical wind Atlas for South Africa. *Energy Procedia*, *76*, 128–922. https://doi.org/10.1016/j.egypro.2015.07.873

Lentz, S. J., & Chapman, D. C. (2004). The importance of nonlinear cross-shelf momentum flux during wind-driven coastal upwelling. *Journal of Physical Oceanography*, *34*(11), 2444–2457. https://doi.org/10.1175/JPO2644.1

Lett, C., Roy, C., Levasseur, A., van der Lingen, C., & Mullon, C. (2006). Simulation and quantification of enrichment and retention processes in the southern Benguela upwelling ecosystem. *Fisheries Oceanography*, *15*(5), 363–372. https://doi.org/10.1111/j.1365-2419.2005.00392.x

Lett, C., Veitch, J., van der Lingen, C., & Hutchings, L. (2007). Assessment of an environmental barrier to transport of ichthyoplankton from the southern to the northern Benguela ecosystem. *Marine Ecology Progress Series*, *347*, 247–259. https://doi.org/10.3354/meps06982

Liu, X., Dunne, J. P., Stock, C. A., Harrison, M. J., Adcroft, A., & Resplandy, L. (2019). Simulating water residence time in the coastal ocean: A global perspective. *Geophysical Research Letters*, *46*(23), 13910–13919. https://doi.org/10.1029/2019GL08509

Lorbacher, K., Dommenget, D., Niiler, P. P., & Köhl, A. (2006). Ocean mixed layer depth: A subsurface proxy of ocean-atmosphere variability. *Journal of Geophysical Research*, *111*(C7), C07010. https://doi.org/10.1029/2003jc002157

Lucas, A. J., Pitcher, G. C., Probyn, T. A., & Kudela, R. M. (2014). The influence of diurnal winds on phytoplankton dynamics in a coastal upwelling system off southwestern Africa. *Deep-Sea Research II*, *101*, 50–62. https://doi.org/10.1016/j.dsr2.2013.01.016

McCabe, R. M., Hickey, B. M., Dever, E. P., & MacCready, P. (2015). Seasonal cross-shelf flow structure, upwelling relaxation, and the alongshelf pressure gradient in the northern California current system. *Journal of Physical Oceanography*, *45*(1), 209–227. https://doi.org/10.1175/JPO-D-14-0025.1

McDougall, T. J., & Barker, P. M. (2011). *Getting started with TEOS-10 and the Gibbs seawater (GSW) oceanographic toolbox* (p. 28). SCOR/IAPSO WG127. ISBN 978-0-646-55621-5.

Monteiro, P., Dewitte, B., Scranton, M., Paulmier, A., & van der Plas, A. (2011). The role of open ocean boundary forcing on seasonal to decadal-scale variability and long-term change of natural shelf hypoxia. *Environmental Research Letters*, *6*(2), 2–18. https://doi.org/10.1088/1748-9326/6/2/025002

Monteiro, P. M. S., & van der Plas, A. K. (2006). Low oxygen water (LOW) variability in the Benguela system: Key processes and forcing scales relevant to forecasting. In L. V. Shannon, G. Hempel, P. Malanotte-Rizzoli, C. L. Moloney, & J. Woods (Eds.), *Benguela: Predicting a large marine ecosystem* (Vol. 14, pp. 71–90). Elsevier, Large Marine Ecosystem Series. https://doi.org/10.1016/s1570-0461(06)80010-8

Ndhlovu, A., Dhar, N., Garg, N., Xuma, T., Pitcher, G. C., Sym, S. D., & Durand, P. M. (2017). A red tide forming dinoflagellate Prorocentrum triestinum: Identification, phylogeny and impacts on St Helena Bay, South Africa. *Phycologia*, *56*(6), 649–665. https://doi.org/10.2216/16-114.1

Nelson, G., & Hutchings, L. (1983). The Benguela upwelling area. *Progress in Oceanography*, *12*(3), 333–356. https://doi.org/10.1016/0079-6611(83)90013-7

Penven, P., Cambon, G., Marchesiello, P., Sepulveda, A., Benshila, R., Illig, S., et al. (2022). CROCO tools (1.3). *Zenodo*. https://doi.org/10.5281/zenodo.7432028

Penven, P., Roy, C., Colin de Verdi´ere, A., & Largier, J. (2000). Simulation of a coastal jet retention process using a barotropic model. *Oceanologica Acta*, *23*, 615–634.

Pitcher, G. C., Aguirre-Velarde, A., Breitburg, D., Cardich, J., Carstensen, J., Conley, D. J., et al. (2021). System controls of coastal and open ocean oxygen depletion. *Progress in Oceanography*, *197*, 102613. https://doi.org/10.1016/j.pocean.2021.102613

Pitcher, G. C., Boyd, A. J., Horstman, D. A., & Mitchell-Innes, B. A. (1998). Subsurface dinoflagellate populations, frontal blooms and the formation of red tide in the southern Benguela upwelling system. *Marine Ecology Progress Series*, *172*, 243–264. https://doi.org/10.3354/meps172253

Pitcher, G. C., & Jacinto, G. S. (2019). Ocean deoxygenation links to harmful algal blooms. D. Laffoley, & J. M. Baxter (Eds.), *Ocean deoxygenation: Everyone's problem - causes, impacts, consequences and solutions, international union for conservation nature, Gland, Switzerland*.

Pitcher, G. C., & Probyn, T. A. (2011). Anoxia in southern Benguela during the autumn of 2009 and its linkage to a bloom of the dinoflagellate Ceratium balechii. *Harmful Algae*, *11*, 23–32. https://doi.org/10.1016/j.hal.2011.07.001

Pitcher, G. C., & Probyn, T. A. (2017). Seasonal and sub-seasonal oxygen and nutrient fluctuations in an embayment of an eastern boundary upwelling system: St Helena Bay. *African Journal of Marine Science*, *39*(1), 95–110. https://doi.org/10.2989/1814232x.2017.1305989

Pitcher, G. C., Probyn, T. A., & du Randt, A. (2022). Changes in water column oxygen, estimates of productivity and the development of anoxia in a major embayment of the southern Benguela eastern boundary upwelling system. *Journal of Marine Systems*, *227*, 103694. https://doi.org/10.1016/j.jmarsys.2021.103694

Pitcher, G. C., Probyn, T. A., du Randt, A., Lucas, A. J., Bernard, S., Evers-King, H., et al. (2014). Dynamics of oxygen depletion in the nearshore of a coastal embayment of the southern Benguela upwelling system. *Journal of Geophysical Research: Oceans*, *119*(4), 2183–2200. https://doi.org/10.1002/2013JC009443

Probyn, T. A., Pitcher, G. C., Monteiro, P. M., Boyd, A., & Nelson, G. (2000). Harmful algal blooms and shellfish mariculture in Saldanha Bay. *South African Journal of Marine Science*, *22*(1), 285–297. https://doi.org/10.2989/025776100784125807

Rouault, M., Pohl, B., & Penven, P. (2010). Coastal oceanic climate change and variability from 1982 to 2009 around South Africa. *African Journal of Marine Science*, *32*(2), 237–246. https://doi.org/10.2989/1814232X.2010.501563

Russo, C. S., Veitch, J., Carr, M., Fearon, G., & Whittle, C. (2022). An intercomparison of global reanalysis products for southern Africa's major oceanographic features. *Frontiers in Marine Science*, *9*, 837906. https://doi.org/10.3389/fmars.2022.837906

Rykaczewski, R. R., Dunne, J. P., Sydeman, W. J., García-Reyes, M., Black, B. A., & Bograd, S. J. (2015). Poleward displacement of coastal upwelling-favorable winds in the ocean's eastern boundary currents through the 21st century. *Geophysical Research Letters*, *42*(15), 6424–6431. https://doi.org/10.1002/2015gl064694

Schmidt, M., & Eggert, A. (2016). Oxygen cycling in the northern Benguela upwelling system: Modelling oxygen sources and sinks. *Progress in Oceanography*, *149*(2016), 145–173. https://doi.org/10.1016/j.pocean.2016.09.004

Schmidtko, S., Stramma, L., & Visbeck, M. (2017). Decline in global oceanic oxygen content during the past five decades. *Nature*, *542*(7641), 335–339. https://doi.org/10.1038/nature21399

Send, U., & Nam, S. (2012). Relaxation from upwelling: The effect on dissolved oxygen on the continental shelf. *Journal of Geophysical Research*, *117*(C4), C04024. https://doi.org/10.1029/2011JC007517

Sharples, J., Middelburg, J. J., Fennel, K., & Jickells, T. D. (2017). What proportion of riverine nutrients reaches the open ocean? *Global Biogeochemical Cycles*, *31*(1), 39–58. https://doi.org/10.1002/2016GB005483

Sydeman, W. J., Garcia-Reyes, M., Schoeman, D. S., Rykaczewski, R. R., Thompson, S. A., Black, B. A., & Bograd, S. J. (2014). Climate change and wind intensification in coastal upwelling ecosystems. *Science*, *345*(6192), 77–80. https://doi.org/10.1126/science.1251635

Tim, N., Zorita, E., Schwarzkopf, F. U., Rühs, S., Emeis, K.-C., & Biastoch, A. (2018). The impact of Agulhas leakage on the central water masses in the Benguela upwelling system from a high-resolution ocean simulation. *Journal of Geophysical Research: Oceans*, *123*(12), 9416–9428. https://doi.org/10.1029/2018JC014218

Tyrell, T., & Lucas, M. I. (2002). Geochemical evidence of denitrification in the Benguela upwelling system. *Continental Shelf Research*, *22*(17), 2497–2511. https://doi.org/10.1016/S0278-4343(02)00077-8

Veitch, J., Penven, P., & Shillington, F. (2009). The Benguela: A laboratory for comparative modelling studies. *Progress in Oceanography*, *83*(1–4), 296–302. https://doi.org/10.1016/j.pocean.2009.07.008

Weeks, S. J., Barlow, R., Roy, C., & Shillington, F. A. (2006). Remotely sensed variability of T and chlorophyll in the southern Benguela: Upwelling frequency and phytoplankton response. *African Journal of Marine Science*, *28*(3–4), 493–509. https://doi.org/10.2989/18142320609504201

Weiss, R. F. (1970). The solubility of nitrogen, oxygen and argon in water and seawater. *Deep-Sea Research and Oceanographic Abstracts*, *17*(4), 721–735. https://doi.org/10.1016/0011-7471(70)90037-9